University of Piraeus

Faculty of Information and Communication Technologies

Department of Digital Systems

MIMO Capacity in Terahertz Band

Master's Thesis

by

Halas Stavros

in partial fulfillment for the completion of

the Master's Program on *Digital Communication & Networks*

Supervisor

Alexiou Aggeliki, Associate Professor

Piraeus, May 2019

Acknowledgements

To this point and by this position I would like to express my sincere gratitude on those who helped me and stood by me during the thesis' completion.

Firstly, I would like to acknowledge the invaluable contribution of my supervisor Alexiou Aggeliki, who has always been abreast and willing to offer time and guidance when was needed. Undoubtedly, her ethos and attitude towards finding creative solutions would be a defining model for now on, as to how to deal with the conflicting demands of an academic environment.

Furthermore, I would also like to thank my friend, colleague and a quite promising young researcher Zerva Maria, whose guidance and critical approach to MATLAB program, allowed me to overcome any difficulties I faced in computer science and was indeed the solid solution I ever needed.

Last but not least, I would like to deeply thank my parents and my brother Stamatis for their ongoing support to all my endeavors up until now, without whom I wouldn't have managed to reach my goals.

Abstract

Chapter 1. Introduction to the Terahertz Band

Chapter 2. Capacity of Massive MIMO Systems in Wireless Communications

Chapter 3. Channel Model and Environment Attenuation in High Frequencies

Chapter 4. Performance Results from GHz to THz for MIMO Simulation

Abstract

The introductory chapter leads the way towards the main steps of the present master's thesis, and its scope is to theoretically address the aim of this thesis, which is to deal with the problems of huge propagation loss and the quite expected laws of attenuation and absorption. In addition, it encircles the study over the THz signaling as well as the communication systems, their foundations, and not only their linear and optics theory but also their utilization in nowadays.

The second chapter examines the literature concerning the capacity of MIMO systems. Apart from that, it provides information about MIMO channel systems and their efficiency, in order to justify its usage in this particular thesis.

The third chapter is concerned about the system channel models and attenuation. Besides that, it introduces the basic physical variable, which is the K-factor, helping with the modeling of these channels, among other ones. The end of this chapter reveals how the atmospheric factors, such as attenuation, re-radiation, spreading, climate, govern telecommunications.

The fourth chapter presents the results of a MIMO experimental simulation, created in the MATLAB environment. Furthermore, it compares the beamforming and multiplexing MIMO capacity of two distinct models: the Hosseini's and the Simplified one. Finally, it outlines state-of-the-art developments relevant to THz communications.

Chapter 1

Introduction to the Terahertz Band

1.1 Overview

The Terahertz band and technology has been increased dramatically over the past twenty years. What is more, the prospects of using THz waves to transmit data have been examined by several teams over the past fifteen years. In combination with new and better THz sources, THz band has become a main laboratory theme as a contemporary mean for exploitation and consequently, several applications have been developed. Indeed, various views of the topic and modulation systems, are covered in a wide range of scientific articles as well as wireless communication measurements have been extendedly reported in the existing bibliography. Nevertheless, this report focuses to the wireless THz communication.

It has been shown that there are diverse descriptions for the THz frequency range. For the purposes of this research, the frequency is set the between 0.3 to 0.5 THz. Furthermore, extreme frequencies for up to 3 THz are also used in order to prove the validity of the model at higher frequencies. However, frequencies of 100 GHz or less are not included although they could according to the literature [1].

Nowadays, the main wireless means to be pointed in microwave communications systems work at carrier frequencies from 20 to 29 GHz [1]. Nonetheless, numerus research projects in the field of electronics that have been carried out for communication systems executing at signals as high as 55 GHz. The radio signals have been found to be reduced in this frequency due to the high oxygen absorption, allowing the creation of low interference picocell mobile communication systems with high capacity [1].

Currently, it is observed that there is a growing request for bandwidth and higher data throughput, specifically for wireless broadband applications. These requirements perhaps are about a broader spectrum access and bandwidth in higher frequency bands. It has been proposed that in the future most demands

for mobile communications are going to deal with a spectrum of less than 5GHz. Nevertheless, it should be noted that the future emerging applications of the THz communications have not been reported to focus on spectrum requirements more than 30 GHz[1]. Particularly, the field between 0.300 to 1.5 THz is suggested to be investigated within the following decade for science and radio services. Even though laboratory work is not taking place at frequencies above 300 GHz, it might do so in the future with applications in fields such as radio astronomy. In the future, a great number of applications are expected to be researched and developed for frequencies above 300 GHz and then the spectrum requirements will be updated [1].

Undeniably, the bandwidth requirements for wireless systems have increased abruptly. In order to meet these demands the spectral utilization efficiency is raised by practicing advanced modulation techniques. That means that point to point data rates, larger number of frequencies within a volume of space and better distribution of the given band of frequencies needed to be increased respectively. Nevertheless, it is observed that there is an upper limit of this plan even when it is operated for a wireless networking in a shared volume of space, achieved by the multi inputs/outputs approaches. Following this observation, transmission bands at higher carrier frequencies must offer the possibility to provide sufficient transmission capacity. Therefore, the requirements for bandwidth in wireless short-range communications have been observed to double every two years over the last 10 years[2]. According to the foresaid, it could be deduced that the data rates will be increased around 10 Gbps in the following years [1].

1.2 Advantages of Terahertz Communication Systems

It has been recognized that the use of THz communication systems with terabit or lower data transmission rates could allow wireless extensions of broadband access fiber optical networks as well as wireless extensions of high speed wired local networks. What is more, they would offer a wireless bridge between lower

[1]For example, above the 25 to 250 GHz, part of the spectrum is expected to be used for radar service and in particular, near 30, 80, 100, and 230 GHz because there are atmospheric problems for transmission.
[2]For example, from less than 1 kbps for wireless telemetry, to more than 200 Mbps with 802.11 wireless local area network in 2018.

data rate wireless local networks and high-speed fiber optical networks. High definition television as well as an improved broadband indoor picocell for mobile users can also be applied due to this technology.

THz communications systems are going to contribute to the improvement of the wireless service but at the same time their existence is going to demand greater bandwidth and therefore, a continuing increase in the carrier frequency for communications and data. However, the high bandwidth dynamics are found to be feasible only with short path length and line-of-sight communication. Currently, the most common optical transmission way for short reach has been the infrared free space communication link at 1.5 μm wavelength. The main way to increasing the infrared wireless data rate to 10 Gbps is the applications of advanced modulation formats, such as orthogonal frequency division multiplexing. In addition, the multiple input multiple output (MIMO) and coherence detection processing has been used to demonstrate a 0.1 Tbps per channel link [2].

In general, the main advantage of THz communication systems compared to microwave or millimeter wave systems is that of higher bandwidth. However, there are some more limitations, such as extremely high data rate requirements over a short distance on a point to point or multipoint to multipoint basis. On one hand, it is claimed that the enormous cost of laying optical cables in big urban centers with high demands for fast internet access is a low probability solution. On the other hand, it is suggested that the nature of THz system would permit it to be adapted to future planning regulations in cities [2].

1.3 Attenuation and Absorption of THz

Free space attenuation is defined as a significant decrease of the signal strength relevant to distance. As a result, the free space attenuation has been suggested to be reduced by the use of actively steerable antennas, which can immensely boost the received signal relative to the weakly directional aerial ones. In addition, the absorption of THz by atmospheric gases limits THz transmission to specific frequency windows. Indeed, molecular absorption, particularly by water vapor has been shown to cause the greatest problems to THz systems and millimeter wave.

Wider spectral bands have been allocated at frequencies from 30 GHz to 100 GHz with a total bandwidth of less than 7 GHz. The bands can support data rates up to 10 Gbps. These advantages are limited to the assigned bandwidth because the Wi-Fi capacity based on some standard which can provide speeds of up to 100 Mbps for 40 MHz bandwidth [2].

There is a variety of international standards organizations which are exploring the technical and operational characteristic of services in the frequency range above 300 GHz. Thus, the THz frequency region offers the potential for the development of systems with much larger bandwidth, ranging from a few GHz to more than 300 GHz [2].

1.4 Millimeter Wave

Although a great number of antennas can be equipped on mobile devices, it is not practical for the current wireless systems that usually work in the 6 GHz spectrum. Moreover, the new generation system (5G) is expected to deliver a massive increase in data rates and channel capacity. There are two main technologies which have attracted lots of attention recently. The first one is the massive multiple input multiple output (MIMO) technology, which advocates in the use of a large number of antennas in wireless communications. The second one is the use of a very high frequency spectrum in the range of 30 GHz to 300 GHz, which is also known as the millimeter wave (mmWave) spectrum. In addition, a short wavelength in mmWave can be used, helping to minimize the inter element spacing of a MIMO system. If the receiver signal strength is fixed to a certain level, then for a given number of transmitter and receiver antennas, the common understanding is that the MIMO capacity is not selective regarding frequency.

It has been reported that there is a type of molecule-induced-re-radiation, often referred to as molecular noise, which is actually highly correlated to the signal waveform due to its re-radiation nature and hence, it can be considered as a distorted copy of the signal from a virtual, non-line form of the sight path. For example, not only water molecules and resonating Oxygen do absorb signal energy causing attenuation, but also they re-radiate some of the absorbed energy. Interestingly, if we consider normal atmosphere, Oxygen and water

molecules will play a major role in the molecular absorption and their natural resonance frequencies are around 60 GHz, 120 GHz, and 180 GHz. It should be noted that the THz communication for cellular networks poses its own challenges, such as high free space path loss and high Doppler shift. Apart from the above factors, another main difference between the existing wireless communication in 6 GHz frequencies and the future one in mmWave is the reaction of the other atmosphere molecules, which can also absorb signal energy if they are excited in their natural resonance frequencies. It has been found that this phenomenon usually occurs in frequencies of the THz spectrum. Last but not least, it has been shown that this molecular re-radiation can change the MIMO capacity performance as it is very similar to scattering which is known to be as highly significant factor, providing spatial diversity to a MIMO channel [3].

Further research concerning the wide range bandwidth from 30 GHz to 300 GHz reveal that the THz communications is about to be an important part of the 5G mobile network worldwide as it can provide multi and gigabit communication services, including high definition television and high definition video. Due to the explosive growth of mobile traffic demand the contradiction between capacity requirements and spectrum shortage become increasingly prominent. Therefore, most of the current research is focused on the 28 GHz band, the 38 GHz band and the 60 GHz band [4].

1.5 Path Loss

Undoubtedly, the increasing demand for the wireless data traffic has become achievable due to the development of the delineated THz band (0.1-10 THz). Currently, the feasible applications of the THz link are limited to short range communications and wireless personal area networks. Although, there is a wide unused bandwidth in this spectrum, the main problem is the high propagation loss when using such spectrum. What is more, the molecular absorption causes loss a part of the radio signal attenuation at the THz frequencies, which is frequency selective and increases the total loss to more than 200 dB from frequencies up to 10 meters distance.

It has been proved that the transmit power is indirectly proportional to the signal path loss, i.e. a significant increase of the former has been found to reduce a

high loss of the signal. Unfortunately, this is limited to a few of mmWave and its application is not feasible to a variety of spectra, at least with the current available technology. Moreover, channel gain can be remarkable improved by means of the multi-antenna beamforming technique. Specially, using a very large-scale MIMO beamforming system has been considered to be applied in the telecommunication field as a practical solution. This is because it can lead to 55 dB channel gain at 1 THz due to the very small footprint of a large number of antennas at the THz band [5].

According to the foresaid, the THz communication is usually assumed to be applied in as a line-of-sight dominant channel because of the huge path loss. Thus, previous research has mainly focused on beamforming rather than multiplexing. Nonetheless, when there is satisfying number of multipath signal components in a rich scattering environment, then the multiplexing system is preferable to the beamforming one. Consequently, the MIMO multiplexing technique is particularly advantageous in such a case [5].

Interestingly enough, numerous theoretical investigations concerning the THz channel capacity for both systems, the multiplexing and beamforming one, in a MIMO set up show that the beamforming technique can provide less capacity gain comparing to the multiplexing technique under the same certain conditions. Furthermore, the multiplexing technique may still be the most preferable choice in other conditions even if the beamforming yields have a higher capacity, due to its easier implementation [5].

1.6 Aim

The purpose of this Thesis is to investigate the capacity of MIMO systems of 300-500 GHz frequencies as well as to explore the main difference between beamforming and multiplexing techniques, which have been thoroughly reviewed in the existing literature. In particularly, the notion of capacity is examined by altering the number of antennas, transmitters and receivers in order to find their relationship. Following, the Hosseini’s and Simplified channel systems models and their attenuation are analyzed by calculating basic physical variables, including the K-factor and the absorption coefficient. Finally, a MIMO experimental simulation, created in MATLAB environment, compares the MIMO

beamforming and multiplexing systems relative to their capacity. In order to calculate the variables, produce the MIMO experimental simulation and graphically depict the generated surfaces, the database of HITRAN is used.

Chapter 2

Capacity of Massive MIMO Systems in Wireless Communications

2.1 Introduction in Wireless Communications

From 1950 to 2000, network capacity was dramatically increased through network densification by a factor of 2700x. During the first decade of 2000, the 4th Generation (4G) Long Term Evolution (LTE) systems kept on paying special attention to network densification and small cells, as an effective approach to increase capacity. What is more, the first standardization efforts on New Radio indicate that the future 5G technology is going to require even more network densification.

Furthermore, a scaled-up version of multiuser MIMO (i.e. massive MIMO-mMIMO) has the potential to further increase network capacity by exploiting the degrees of freedom in the spatial domain. Indeed, mMIMO has been adopted as a main technology to improve area spectral efficiency (ASE) in 5G systems. However, the larger the number of antennas, the larger the number of degrees of freedom and therefore, the more the multiplexing opportunities. In addition, when time division duplex (TDD) systems are considered, because of a finite channel coherent time, the performance of mMIMO systems may be limited by inaccurate channel state information (CSI). As a result, pilot contamination is considered as a major obstacle, occurring when the same set of uplink training sequences is re-used across neighboring cells [6].

Looking at mMIMO deployment aspects, a better performance can be achieved by increasing the number of antennas at the base station and using a simple signal processing. The uplink signal to interference plus noise ratio (SINR) and rate performance in a mMIMO system, have been analyzed so as to implement a single slope path loss model, without differentiating line-of sight (LoS) and no-line-of-sight (NLoS) transmission [6].

2.2 Capacity with Channel Model

Consider a transmitter with M transmit antennas and a receiver with N receive antennas. Then, the channel can be represented by the $N \times M$ matrix H of channel gains H_{ij} representing the gain from transmit antenna j to receive antenna i. Thus, $N \times 1$ received signal y is equal to:

$$y = Hx + n_r \tag{2.1}$$

Where x is the $M \times 1$ transmitted vector and n is the $N \times 1$ addictive white circularly symmetric complex gaussian noise vector, normalized so that its covariance matrix is the identity matrix. The normalization of any non-singular noise covariance matrix K_w to fit the above model is as straightforward as multiplying the received vector y with ${K_w}^{-\frac{1}{2}}$ to yield the effective channel ${K_w}^{-\frac{1}{2}}H$ and a white noise vector. Thus, the channel state information is the channel matrix H.

The transmitter is assumed to be subject to an average power constraint of P across all transmit antennas for example, $E[x^H x] \leq P$. Then, the noise power is normalized to unity, and to refer to this power constraint P as SNR. There are two main perfect choose, first is the perfect receiver channel state information (CSIR) and transmitter channel state information (CSIT) and second is the perfect CSIR and transmitter channel distribution information (CDIT) [7].

Moreover, with perfect CSIT or CSIR, the channel matrix H is assumed to be known perfectly and instantaneously at the transmitter or receiver, respectively. In addition, when the transmitter or receiver knows the channel state perfectly, it knows the distribution of this state perfectly, since the distribution can be obtained from the state observation [7].

On the other hand, the perfect CSIR and CDIT models are motivated by the scenario where the channel state can be accurately tracked at the receiver and the statistical channel model at the transmitter is based on the channel distribution information fed back from the receiver. Therefore, this distribution model is typically based on receiver estimates of the channel state and the uncertainty and delay associated with these estimates. The following figure (2.1)

shows that the underlying communication model of the scenario, where $\tilde{N}$ denotes the complex gaussian distribution [7].

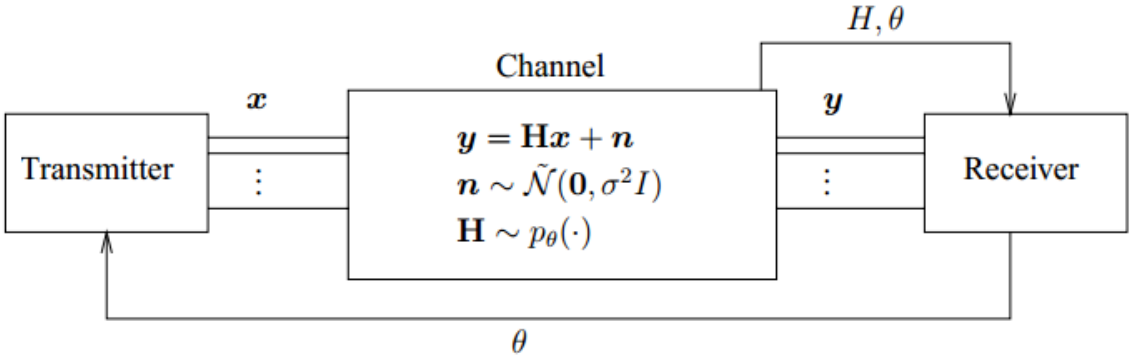

Figure 2.1 MIMO channel with perfect CSIR. Taken by [7].

2.3 Multiple Input Multiple Output Capacity

For a simple input multiple output (Simo) flat fading wireless channel, the input/output relations per channel that can be used are modelled by the complex baseband notation by the equation 2.1. Where y represents a single realization of the multivariate random variable Y, h represents the complex channel vector between a single transmit antenna, $\mathrm{N_R}$ receive antennas (for example $\mathrm{h} = \left[\mathrm{h}_{11}, \mathrm{h}_{21}, \ldots, \mathrm{h}_{\mathrm{n_R}1}\right]^{\mathrm{T}}$), x represents the transmitted complex symbol per channel use and n represent a complex additive white gaussian noise vector.

Furthermore, with $\mathrm{h_d}(.)$ denoting differential entropy (entropy of a continuous random variable), the mutual information may be expressed as:

$$\begin{aligned} \mathrm{I(X;Y)} &= \mathrm{h_d(Y)} - \mathrm{h_d(Y|X)} \\ &= \mathrm{h_d(Y)} - \mathrm{h_d(hX + N|X)} \\ &= \mathrm{h_d(Y)} - \mathrm{h_d(N|X)} \\ &= \mathrm{h_d(Y)} - \mathrm{h_d(N)} \end{aligned} \tag{2.2}$$

Thus, it will be assumed that $\mathrm{N}\sim\mathrm{N}(0, \mathrm{K^n})$, where $\mathrm{K^n} = \mathrm{E}\{\mathrm{NN^H}\}$ is the noise covariance matrix. However, the normal distribution maximizes the entropy over all distributions with the same covariance and the mutual information is maximized when $\mathrm{Y}\sim\mathrm{N}(0, \mathrm{K^y})$ where $\mathrm{K^y} = \mathrm{E}\{\mathrm{YY^H}\}$ is the covariance matrix of the desired signal.

Research concerning the complex gaussian vector Y shows that the differential entropy is less than or equal to $\log_2 \det(\pi e K^y)$, with equality if and only y is a circularly symmetric complex gaussian with $E\{YY^H\} = K^y$. Assuming that the assumption that the signal X is uncorrelated with all elements in N, the received covariance matrix K^y may be expressed as [8]:

$$E\{YY^H\} = K^y = E\{(hX + N)(hX + N)^H\}$$

$$= \sigma_x^2 hh^H + K^n \tag{2.3}$$

Where $\sigma_x^2 = E\{X^2\}$.

Furthermore, the SIMO fading channel capacity is:

$$C = h_d(Y) - h_d(N)$$

$$= \log_2 \left[\det\left(\pi e(\sigma_x^2 hh^H + K^n)\right)\right] - \log_2[\det(\pi e K^n)]$$

$$= \log_2[\det(\sigma_x^2 hh^H + K^n)] - \log_2[\det K^n]$$

$$= \log_2 \left[\det\left((\sigma_x^2 hh^H + K^n)(K^n)^{-1}\right)\right]$$

$$= \log_2\left[\det\left(\sigma_x^2 hh^H (K^n)^{-1} + I_{n_R}\right)\right]$$

$$= \log_2\left[\det\left(I_{n_R} + \sigma_x^2 (K^n)^{-1} hh^H\right)\right]$$

$$= \log_2 \left[\left(1 + \frac{P_R}{\sigma_n^2}\|h\|^2\right)\det\left(I_{N_R}\right)\right]$$

$$= \log_2 \left(1 + \frac{P_r}{\sigma_n^2}\|h\|^2\right) \tag{2.4}$$

Where it is assumed that $K^n = \sigma_n^2 I_{N_R}$ and, $\sigma_x^2 = P_R$. Thus, for SISO fading channel, $K^n = \sigma_n^2$. The capacity formula for SIMO fading channel could have been found by assuming maximum ratio combined to the receiver. With perfect channel knowledge at the receiver, the optimal weights are given by [2]:

$$W_{opt} = (K^n)^{-1} h \tag{2.5}$$

Using these weights together with the assumption that $K^n = \sigma_n^2 I_{N_R}$, the overall SNR is γ_T for the current observed channel h is equal to:

$$\Gamma_T = \frac{P_R}{\sigma_n^2}\|h\|^2 \tag{2.6}$$

If, γ_t represents the maximum available SNR, the capacity can be written as:

$$C = \log_2(1 + \gamma_T) = \log_2 \left(1 + \frac{P_r}{\sigma_n^2}\|h\|^2\right) \tag{2.7}$$

In the special case of MIMO capacity, the input/output relation per channel use of a MIMO flat fading wireless channel can be calculated by the complex baseband equation 2.1. Where x is the $(n_T \times 1)$ transmit vector, y is the $(n_R \times 1)$ receive vector, H is the $(n_T \times n_R)$ channel matrix and n is the $(n_R \times 1)$ additive white gaussian noise vector.

$$H = \begin{bmatrix} h_{11} & \dots & h_{1n_T} \\ h_{21} & \dots & h_{2n_T} \\ \vdots & \ddots & \vdots \\ h_{n_R1} & \dots & h_{n_Rn_T} \end{bmatrix} \tag{2.8}$$

In addition, with $h_d(.)$ denoting differential entropy (entropy of a continuous random variable), the mutual information may be expressed as:

$$\begin{aligned} I(X;Y) &= h_d(Y) - h_d(Y|X) \\ &= h_d(Y) - h_d(HX + N|X) \\ &= h_d(Y) - h_d(N|X) \\ &= h_d(Y) - h_d(N) \end{aligned} \tag{2.9}$$

It can be assumed that, $N \sim N(0, K^n)$. Since the normal distribution maximizes the entropy over all distributions with the same covariance, the mutual information is maximized when Y represents a multivariate gaussian random variance. With the assumption that X and N are uncorrelated, the received covariance matrix K^y may be expressed as:

$$\begin{aligned} E\{YY^H\} = K^y &= E\{(HX + N)(HX + N)^H\} \\ &= HK^xH^H + K^n \end{aligned} \tag{2.10}$$

Where, $K^x = E\{XX^H\}$.

Furthermore, the MIMO fading channel capacity is given by the following equation:

$$\begin{aligned} C &= h_d(Y) - h_d(N) \\ &= \log_2\left[\det\left(\pi e(HK^xH^H + K^n)\right)\right] - \log_2[\det(\pi eK^n)] \\ &= \log_2[\det(HK^xH^H + K^n)] - \log_2[\det K^n] \\ &= \log_2\left[\det\left((HK^xH^H + K^n)(K^n)^{-1}\right)\right] \end{aligned}$$

$$= \log_2\left[\det\left(\mathrm{HK^xH^H}(\mathrm{K^n})^{-1} + \mathrm{I_{N_R}}\right)\right]$$

$$= \log_2\left[\det\left(\mathrm{I_{N_R}} + (\mathrm{K^n})^{-1}\mathrm{HK^xH^H}\right)\right] \quad (2.11)$$

When the transmitter has no knowledge of the channel, it is optimal to evenly distribute the available power $\mathrm{P_T}$ among the transmit antennas. Then, $\mathrm{K^x} = \frac{\mathrm{P_T}}{\mathrm{N_T}}\mathrm{I_{n_T}}$. Assuming that the noise is uncorrelated between branches, the noise covariance matrix is $\mathrm{K^n} = \sigma_\mathrm{n}^2\mathrm{I_{n_R}}$. Thus, the MIMO general capacity formula that is shared between the receiver and the transmitter can be found by the equation:

$$C_{general}^{MIMO} = \log_2\left[det\left(I_{N_r} + \frac{\mathrm{P_T}}{\mathrm{N_T}\sigma_\mathrm{n}^2}Hxx^*H^*\right)\right] \quad (2.12)$$

Where HH^* is the identity matrix multiplied by the eigenvalues at each 1 position, $\mathrm{P_T}$ is the transmitting power of transceiver, I is the identity matrix,$xx^* \to I_{N_R} \to 1$, N_R is the number of receivers and N_T is the number of transmitter. However as N_T becomes larger and N_R is fixed. Therefore, $\frac{\mathrm{P_T}}{\mathrm{N_T}\sigma_\mathrm{n}^2}HI_{N_r}H^* \to \frac{\mathrm{P_T}}{\mathrm{N_T}\sigma_\mathrm{n}^2}HH^* \to \frac{P_T}{\sigma_n^2} \to tr(H)$ because $\frac{1}{\mathrm{n_T}}\mathrm{HH^H} \to \mathrm{I_{n_R}}$. Where λ_I denotes singular values of the matrix H (sum of -1*entropies), and hence the squared singular values λ_i^2 denotes the eigenvalues of the matrix $\mathrm{HH^H}$. Also, k denotes the number of non-zero, λ_i^2, which is called the rank of H with $\mathrm{k} \le \min(\mathrm{N_R}, \mathrm{N_T})$, So, $tr(H) = \sum\lambda_i$. Then the multiplexing capacity is calculating:

$$C_{Multiplexing} = \log_2\prod_{i=1}^{N_r}(1+\lambda_i) = \sum_{i=1}^{N_r} log_2(1+\lambda_i) \quad (2.13)$$

But the ergodic capacity is always greater than the rate of transitions.

$$C_{ergodic} = \mathbb{E}\left[\log_2\left(det\left(I_r + \frac{\gamma}{N_T}HH^*\right)\right)\right] \quad (2.14)$$

Where $\gamma = \mathbb{E}[SNR] \sim SNR$ (used in coding) which is the main difference between beamforming and multiplexing. Consequently, $tr(H) = \sum\boldsymbol{\gamma}\lambda_i$. Accepting the same assumptions for the beamforming capacity:

$$C_{Beamforming} = \sum_{i=1}^{N_r} log_2(1+\gamma\mathbb{E}[|x_i|^2]\lambda_i) = \sum_{i=1}^{N_r} log_2(1+\boldsymbol{\gamma}\lambda_i) \quad (2.15)$$

Where $\mathbb{E}[|x_i|^2] = 1$.

The normalized capacity depends on minimum capacity of each one:

$$C_{norm} = \frac{C}{min(N_T, N_R)} \quad (2.16)$$

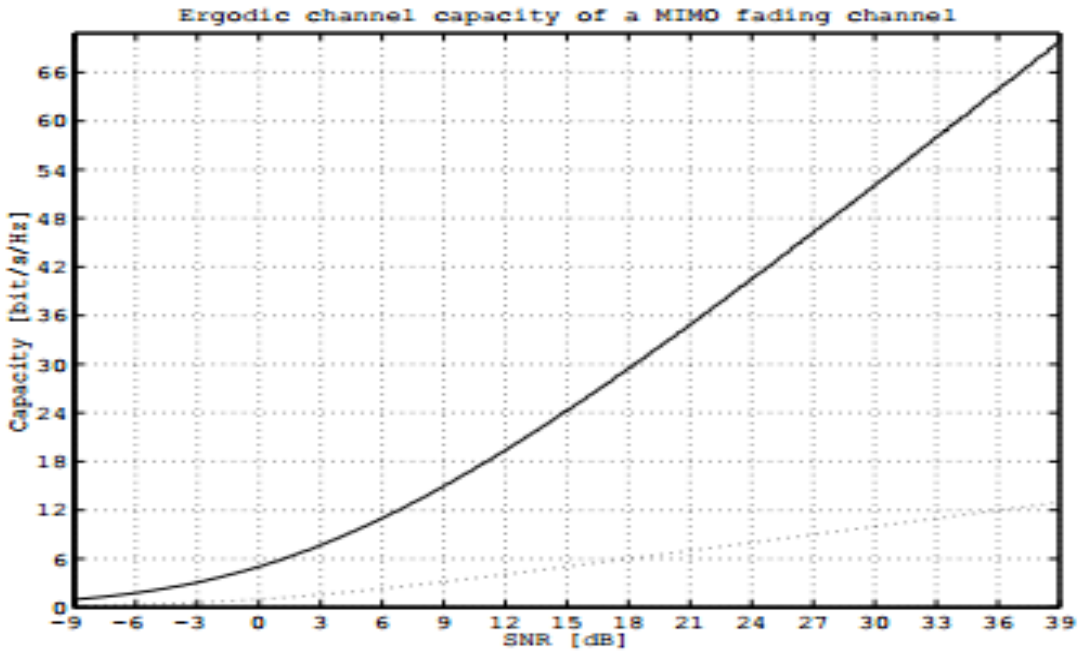

Figure 2.2 The Shannon capacity of a SISO channel compared to the ergodic capacity of a Rayleigh fading MIMO channel. Taken by [8].

2.4 MISO, SIMO and MIMO Comparison of Capacity

The capacity of SISO and MIMO systems in terms of signal to noise ratio (SNR) for several values of N_R and N_T has been graphically represented in previous research (figure 2.3). Specifically, in the SISO case (for N_R=1 and M=1) capacity ranges from 1 to 17 bps per Hz. It can be seen that SISO remains low and increases slowly with the SNR, illustrating the limitations of SISO transmissions. The current techniques to make the most of a SISO channel capacity remain limited and a multi antenna system gets better performance. However, in case MIMO case (for N_R=4 and N_T=4) capacity ranges from 3 to 48 bps per Hz and it is 3 times larger than SISO. As a result, MIMO increases rapidly with the SNR, illustrating the performance of a MIMO communication [9].

In addition, the relationship between MIMO capacity to the number of antennas is illustrated in the figure 2.4. It reveals that MIMO capacity grows linearly with respect to the number of antennas and it is approximately N_T times larger than SISO capacity. Moreover, the performance gain for MISO has been found to be

negligible when the number of transmit antennas increases. Apart from that, it has been proved that the SIMO system is more efficient than the SISO and the MIMO system which ranges from 1 to 3.4 bps per Hz. Consequently, it can be deduced that performance remains low for a limited number of antennas, showing the limitations of SISO and MISO transmissions. Thus, further research can focus on comparing the variations of capacity of SIMO and MIMO systems based on the number of antennas for a constant SNR value. It would be expected that the higher the SNR value is, the better the capacity would be [9].

The main advantage in terms of capacity of MIMO systems is because of the exploitation of multipath. Multipaths allow the receiver to distinguish the different transmitting antennas and then, to simultaneously transmit multiple symbols. Furthermore, another advantage of multipath MIMO system is that each path is a replica of the transmitted signal and then, carrying useful information. Last but not least, each path in such a system is equivalent to the direct signal emitted by a virtual antenna, which can potentially increase the number of transmit antennas. Nevertheless, there is a downside for such high capacity system which is the price, as costly first material is required in order to proliferate the antennas and their associated electronics [9].

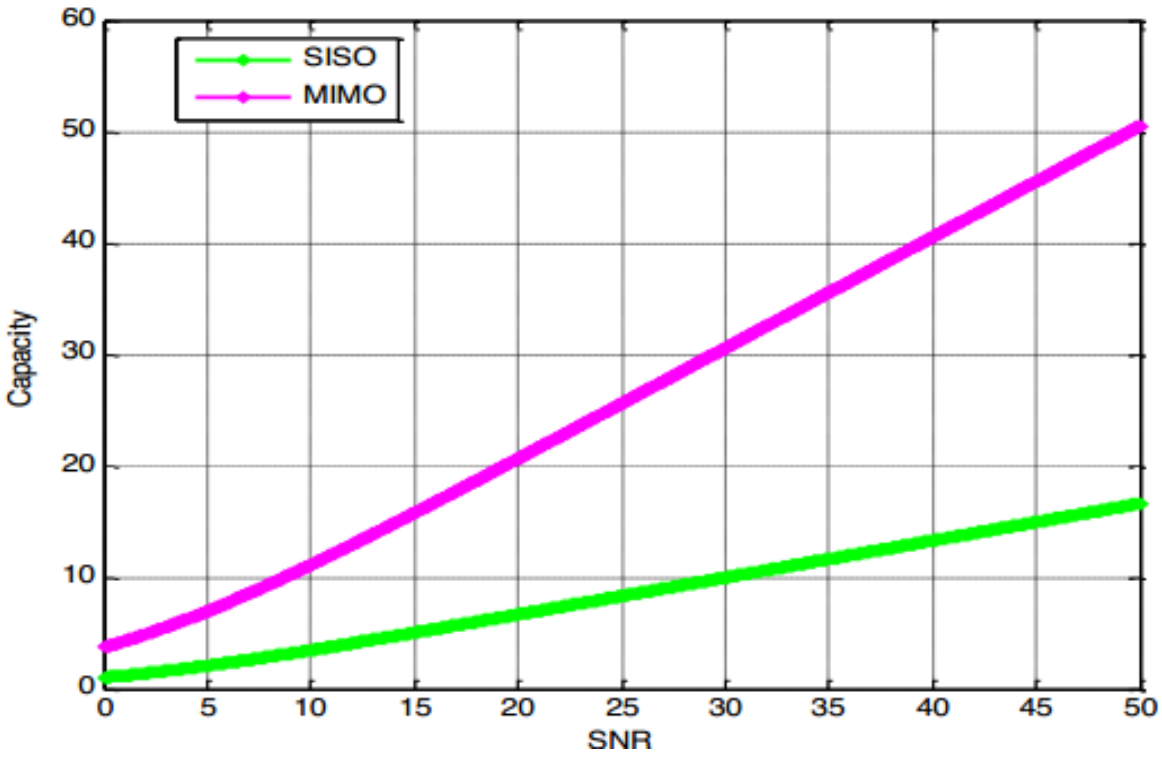

Figure 2.3 The increase of capacity according to SNR between SISO and MIMO. Taken by [9]

The following figure shows that the MIMO capacity is directly proportional to the SNR. For three pairs of antennas: first $(N_T = N_R = 2)$ and $(N_T = N_R = 3)$, second $(N_T = N_R = 4)$ third $(N_T = N_R = 6)$ and $(N_T = N_R = 8)$, it is revealed that MIMO capacity is doubled and then, rapidly increases as the SNR increases, with a gain of more than 50% at 20 dB SNR. As a result, a gain of more than 70% at 20 dB SNR would be expected for the pair of antennas $(N_T = M_R = 8)$ and $(N_T = M_R = 12)$ [9].

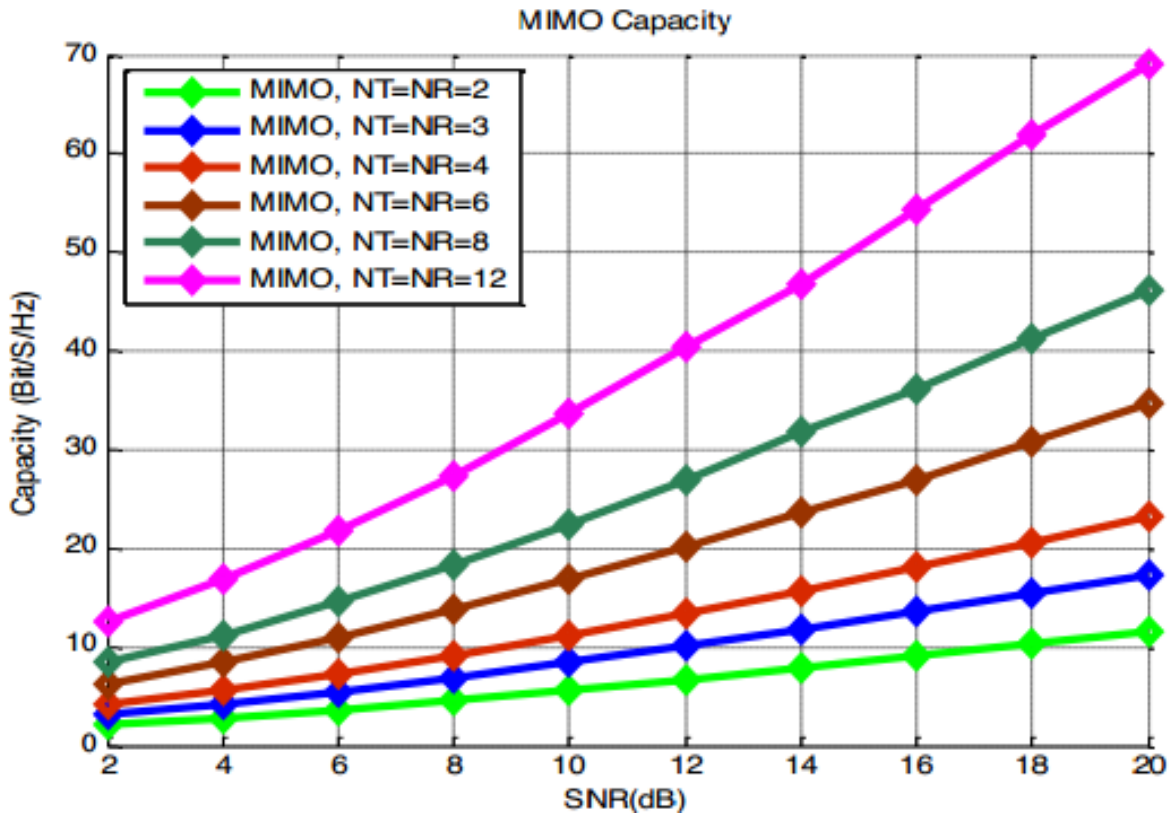

Figure 2.4 Increasing the number of antennas for many MIMO systems capacity increases. Taken by [9]

2.5 MIMO Capacity as a Function of Antenna Number

It has been confirmed that one of the key benefits about the communication around [50-150] GHz is its potential incorporation with the mMIMO technology to generate a tremendous MIMO capacity. The molecular absorption effect on the MIMO capacity for a large number of antennas is shown in the following figure (2.5). By observing the following figure, it can be inferred that the MIMO capacity increases as the number of both receiver and transmitter antennas increases. Thus, the development of this particular MIMO simulation system was based on the parameter values given in the Table I except the array angles θ and φ, which

were chosen randomly. The experiment was repeated 5000 times and the average results for frequencies of 50, 55, 60, 65, 70 GHz is illustrated in figure 2.5 [3].

As far as the molecular absorption is concerned, the MIMO capacity increases linearly as the number of antennas increases. However, capacity gain is much more obvious for frequencies 55 to 65 GHz around the natural resonance frequency of Oxygen. This is because oxygen creates an opportunistic spectrum window for high-efficiency MIMO communications in mmWave. On the other hand, in the absence of molecular absorption, the MIMO capacity is non-selective to frequency although it does increase with the number of antennas because of the dominant LoS transmission [3].

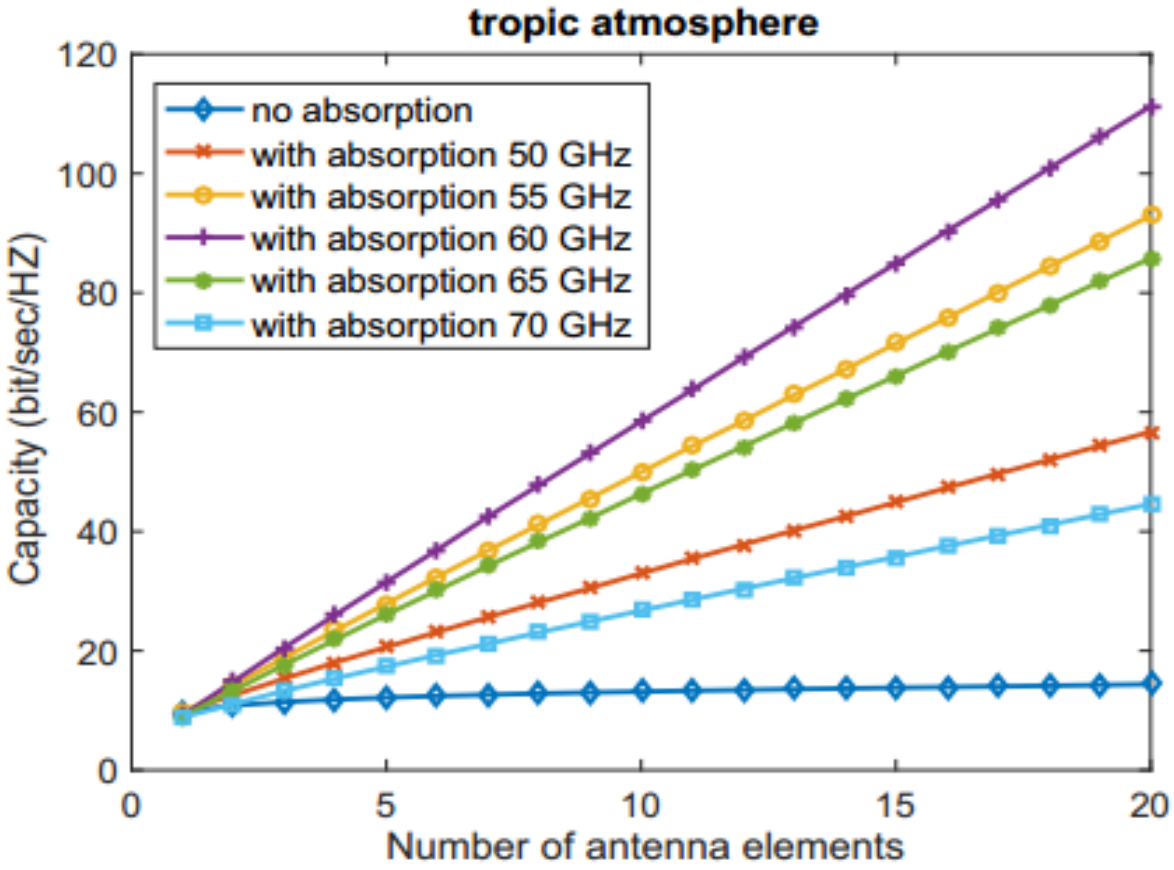

Figure 2.5 MIMO capacity increases linearly as the antenna number increases. Taken by [3]

Chapter 3

Channel Model and Environment Attenuation in High Frequencies

3.1 Different Values of K-Factor

The index K-factor functions as a measure of the probable presence of natural or anthropogenic solid, liquid or gas opaque to semi-opaque obstacles and the physical metric or common Euclidean distance between Tx/transmitter(s) and Rx/receiver(s) assuming non-empty atmospherics or, equivalently, the presence of a typical earthly atmosphere both in total and partial gas pressures and approximately in composition, with:

$$K_{factor} = \frac{e^{-A_{abs}(f)\cdot d}}{1-e^{-A_{abs}(f)\cdot d}} \tag{3.1}$$

where d is the distance between one transmitter and one receiver and $k(f)$ is the total molecular absorption coefficient in frequency f:

$$A_{abs}(f) = \sum_{n=1}^{N} m_n A_{abs_n}(f) \tag{3.2}$$

where each $A_{abs_n}(f)$ is the (partial) molecular absorption coefficient of each gas of accepted atmospheric/propagation model at frequency f and m_n appropriate weight coefficients. So:

$$K_{factor} = \frac{e^{-d\cdot\sum_{n=1}^{N} m_n A_{abs_n}(f)}}{1-e^{-d\cdot\sum_{n=1}^{N} m_n A_{abs_n}(f)}} = \left(e^{d\cdot\sum_{n=1}^{N} m_n A_{abs_n}(f)} - 1\right)^{-1} \tag{3.3}$$

A vital connection to attenuation absorption coefficients is:

$$K_{factor}(f,d) = \frac{e^{-A_{abs}(f)\cdot d}}{1-e^{-A_{abs}(f)\cdot d}} = \frac{e^{-A_{abs}(f,d)}}{1-e^{-A_{abs}(f,d)}} \tag{3.4}$$

for the attenuation absorption coefficient:

$$A_{abs}(f,d) = e^{A_{abs}(f)\cdot d} = \frac{1}{\tau(f,d)} \tag{3.5}$$

or:

$$K_{factor}(f,d) = \frac{e^{-A_{abs}(f)\cdot d}}{1-e^{-(A_{abs}f)\cdot d}} = \frac{e^{-\frac{A^2_{spread}(f,d)A_{abs}(f)c}{4\pi f}}}{1-e^{-\frac{A^2_{spread}(f,d)A_{abs}(f)c}{4\pi f}}} = K_{factor}(f) \tag{3.6}$$

For the attenuation spreading coefficient $A_{spread}(f,d) = \left(\frac{4\pi f d}{c}\right)^2$.

However, the equation (3.2) according to the theory of spectroscopy can be written as [10]:

$$A_{abs}(f) = \sum_{n=1}^{N} \frac{T_{stp}}{P_{stp}} \frac{P^2}{T^2} \frac{N_A}{R} \frac{f^2}{f_c^2} \frac{tanh\left(\frac{h_c f}{2k_B T}\right)}{tanh\left(\frac{h_c f_c}{2k_B T}\right)} \frac{a_L}{\pi} \left[\frac{1}{(f-f_c)^2+a_L^2} + \frac{1}{(f+f_c)^2+a_L^2}\right] \quad (3.7)$$

Where:

$$a_L = \left[(1-q)a_{0,air} + qa_0\right]\left(\frac{P}{P_{stp}}\right)\left(\frac{T_{stp}}{T}\right)^{\delta} \quad (3.8)$$

Where f is the frequency, f_c is the carrier frequency, T is system temperature (for Kelvin is 273.15 + current temperature), P is system pressure, T_{stp} is the standard temperature, P_{stp} is the standard pressure, N_A is Avogadro constant, R is Gas constant, c is light speed, k_B is Boltzmann constant, h is Planck constant, δ is the linear pressure shift (which is usually valued between 0.33 to 0.97), q is the weather carries the atmospheric model from Table II (where Table II shows USA model for mean latitude for summer and winter, high latitude for summer and winter as well as for tropics), a_L is lorez half-width from [11], then a_0 is lorez half-width for normal condition and $a_{0.air}$ is lorez half-width for the air. The absorption coefficient vector can be calculated by the equation 3.7 by substituting all the constants and by changing frequency, temperature and pressure for 5 different atmospheric models. As a result, from (3.1) and given that d is the pre-determined space distance between 0.1 to 10-meter, the K-factor is calculated, allowing to develop the simulation of this Thesis [10], [11].

3.2 Channel Modelling and Capacity Analysis

A channel model is an essential piece of a physical layer communication simulation. It is a mathematical representation of the effects of a communication channel, through which wireless signals are propagated. The channel model is the impulse response of the channel medium in the time domain or, equivalently, its Fourier transform in the frequency domain. In general, the channel impulse response of a wireless communication system varies randomly over time [12].

By utilizing the right channel model in a (tele) communications design, link performance, system architecture tradeoffs performance and provision of a realistic assessment of the overall system performance can be optimized. Many factors are considered in creating a channel model, such as carrier frequency, bandwidth, the locations of transmitter and receiver, Doppler frequency, medium type, polarization, weather conditions and noise types. Selecting a channel model is a tradeoff between computational efficiency and model complexity [12].

3.3 A Simplified Channel Model in the 275-400 GHz

The amount of radiation at frequency f and distance d capable of propagating through the medium without being lost, using the Beer Lambert Law is the transmittance [13]:

$$\tau(f,d) = \frac{P_{Rx}(f,d)}{P_{Tx}(f)} \tag{3.9}$$

that can be reformulated as:

$$\tau(f,d) = e^{-\sum_{i=1}^{N} A_{abs_i}^{\alpha}(f)d} \tag{3.10}$$

It is a function of both frequency and distance. Where f is the frequency of the travelling wave and d the distance between the transmitter and receiver antennas. The absorption coefficient (A_{abs}) at f is the summand for all individual molecule absorptions. $P_{Rx}(f)$, $P_{Tx}(f)$ in Watt are the received and transmitted signal powers respectively. Equation 3.10 is the foundation of THz research, because molecular absorption loss, frequency-distant dependent noise and receiver noise temperature are directly derived by it. Transmittance is dimensionless and its maximum value never exits one. To better comprehend its physical meaning, one could view it as a percentage by multiplying it with 100 % [13].

THz channel model can be easily estimated by calculating the absorption coefficient, using HITRAN parameters, but it is cumbersome as it involves many complicated equations. Furthermore, the novel model of molecular absorption loss in the region of 275 - 400 GHz, firstly presented in equation 3.8, yields results almost similar to those obtained using the HITRAN database and therefore, proves the validity of the former model [11], [13].

According to the foresaid, the THz channel model for the particular frequency range (equation 3.13) is presented. It is known that the current absorber of electromagnetic (EM) wave energy at THz band transmissions is the atmospheric water vapor, which dominates the loss above 200 GHz. In order to evaluate the molecular absorption loss in the 275 - 400 GHz band a Simplified model for molecular absorption due to water vapor is utilized [13].

The absorption coefficient for the Simplified model can be calculated from [14]:

$$A_{abs}(f) = y_1(f,\mu) + y_2(f,\mu) + g(f) \tag{3.12}$$

and firstly, by using the equation 3.10 and then the equation 3.12 the molecular absorption gain is estimated as:

$$G_{A_{abs}}(f,d) = e^{-d\left(y_1(f,\mu)+y_2(f,\mu)+g(f)\right)} \tag{3.13}$$

Where μ denotes the volume mixing ratio of water vapor. Water vapor is conflicted with relative humidity and is given by:

$$\mu = \frac{\varphi p_w^*(T,p)}{100p} \tag{3.14}$$

Where φ stands for the relative humidity as a percentage and p for the atmospheric pressure in hPa. Whereas, the saturated water vapor partial pressure $p_w^*(T,p)$ at temperature T can be calculated according to the Buck equation [14], [15].

The parameters of the equation 3.13 can be given by the following equations:

$$y_1(f,\mu) = \frac{A(\mu)}{B(\mu)+\left(\frac{f}{100c}+c_1\right)^2} \tag{3.15}$$

$$y_2(f,\mu) = \frac{C(\mu)}{D(\mu)+\left(\frac{f}{100c}+c_2\right)^2} \tag{3.16}$$

$$g(f) = p_1 f^3 + p_2 f^2 + p_3 f^1 + p_4 \tag{3.17}$$

Where, $c_1 = 10.835\ cm^{-1}$, $c_2 = 12.664\ cm^{-1}$, $p_1 = 5.54 \times 10^{-37}\ Hz^{-3}$, $p_2 = -3.94 \times 10^{-25}\ Hz^{-2}$, $p_3 = 9.06 \times 10^{-14}\ Hz^{-1}$, $p_4 = -6.36 \times 10^{-3}$,

$$A(\mu) = 0.2205\mu(0.1303\mu + 0.0294) \quad (3.18)$$

$$B(\mu) = (0.1303\mu + 0.0294)^2 \quad (3.19)$$

$$C(\mu) = 2.014\mu(0.1702\mu + 0.0303) \quad (3.20)$$

$$D(\mu) = (0.537\mu + 0.0956)^2 \quad (3.21)$$

This model was shown to be very accurate to distances up to 1 km in standard atmospheric conditions (temperature 296 K and air pressure 1 atm). In addition, it is evident from the equation 3.13 that this model can describe molecular absorption pathloss at conditions beyond of the standard. Moreover, it should be noted that c1, c2 , p1, p2, p3 and p4 are considered relatively independent of the atmospheric conditions [14].

If the set of known equations is modified, including the general pathloss equation, the absorption coefficient equation, the pathloss due-to-excess-of-water equation, then the following graph can be obtained by applying the equation:

$$PL\left(f, d, \mu_{H_2O}\right) = e^{d(y_1+y_2+g)} \quad (3.22)$$

Where y_i is the function of f, μ_{H_2O} and g of f [14].

The purpose of introducing the Simplified channel model was to find a valid model at the 0.275–0.4THz frequency band. However, as it can be computationally proven, the model is equally accurate from 0.250 to 0.375 THz. From the graph 3.1, it can be observed that the available bandwidth decreases as a function of frequency and as a function of distance, which is related to the exponential molecular absorption loss. It has been proposed that the numerical model is very useful for millimeter and low terahertz band communications analysis.

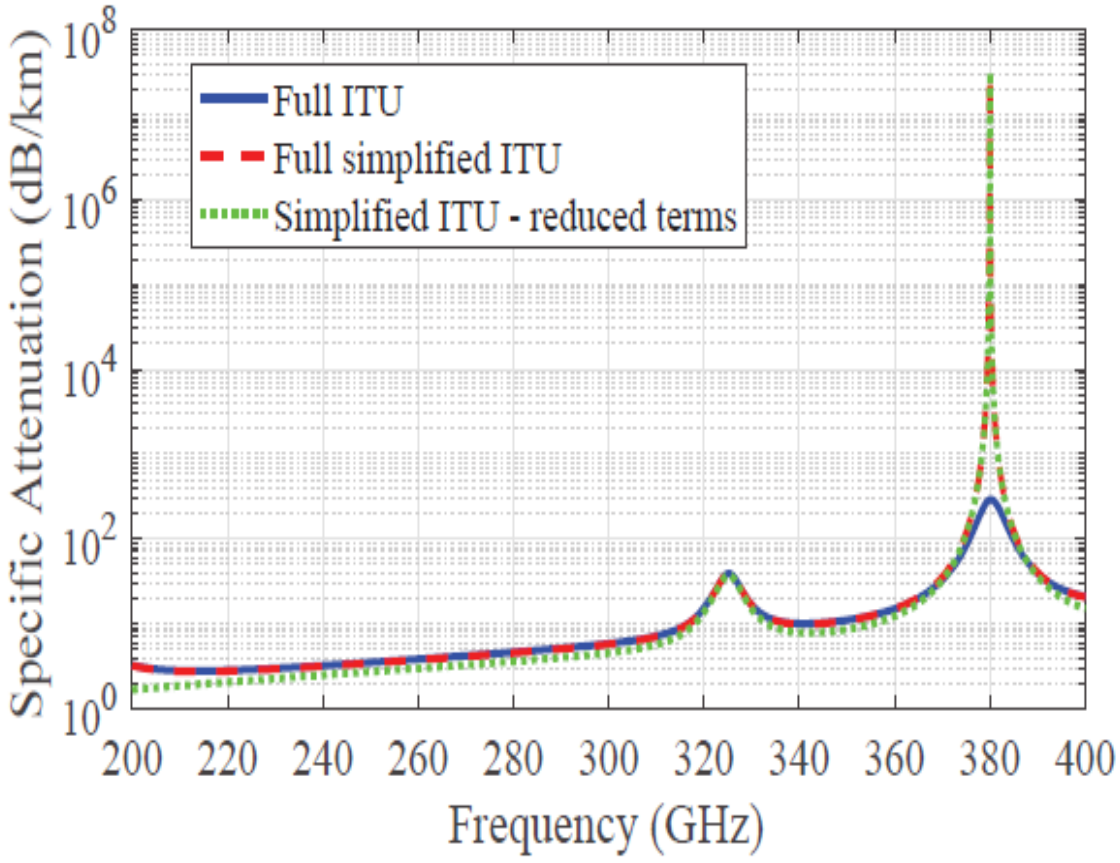

3.1 Information about a Simplified channel model for modeling the absorption coefficient in the 0.275 – 0.4 THz band. Taken by [14]

3.4 Atmospheric Molecular Absorption

It is known that there would be a loss in signal during its propagation through the atmosphere. This is because the molecules present in it have resonance frequencies at which high losses occur. Most of the times, the loss of signal for a typical temperature in the atmosphere varies according to the water vapor content in it. In particular, it has been found that for frequencies above 10 GHz, the loss rises steadily until a frequency of about 60 GHz is reached. At this frequency, the atmospheric loss increases sharply. The large absorption peak above 60 GHz is confirmed to be due to the absorption of oxygen and dry air. This is depicted in figure 3.2, where the value of attenuation is plotted on a logarithmic scale and tends to compress in the extreme values of loss. This figure also illustrates the loss per kilometer against frequency for both vertical and horizontal polarization for a peak rain rate of 40 mm/h [16].

Rain, snow and hail have thus been found to hinder the propagation of mmWaves. Specifically, in rain it has been proved that there is a high correlation between absorption and frequency. Therefore, when planning methods for services such as broadcasting and mobile communications, attenuation of the signals can be easily overcome by altering the frequency. However, for fixed links at frequencies of above 20 GHz, it is often the most significant factor in limiting the maximum possible path length. The effect of rain also depends on the rainfall rate. Statistics have revealed that the most significant value of the rainfall rate in a region is the peak one, rather than the total annual rainfall. So, it is normally for when designing a radio link, it for a certain percentage unamiability, usually 0.01% for a particular time and it does not necessarily relate directly to annual rainfall [16].

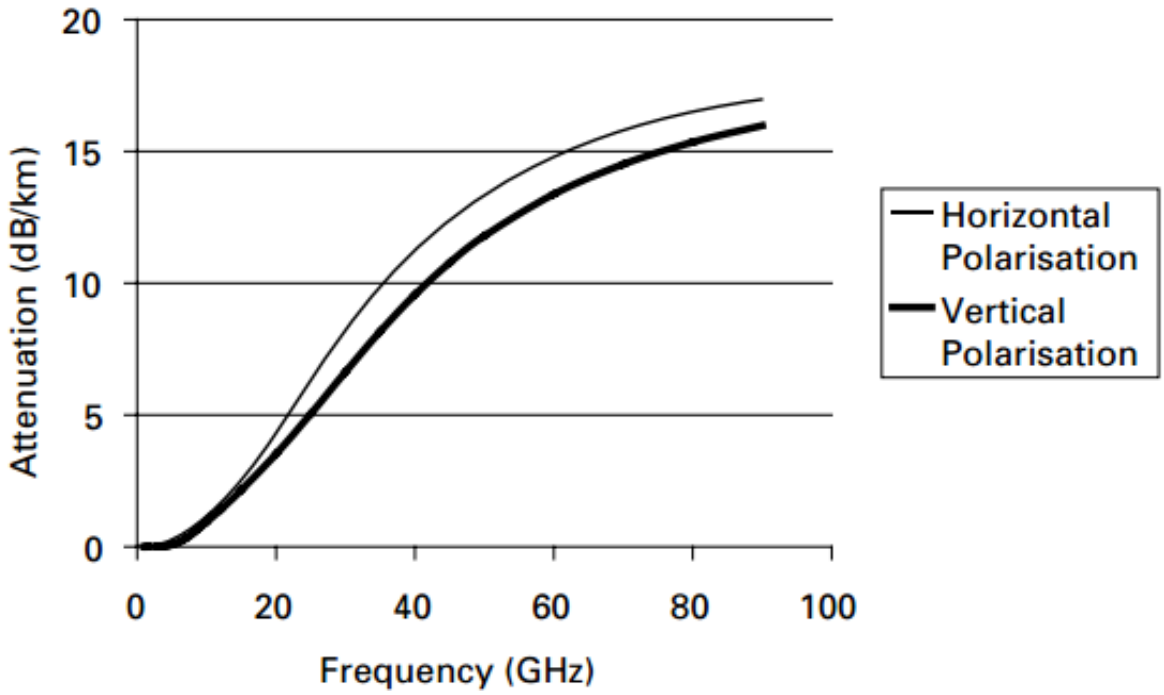

Figure 3.2 The path loss with frequency for a rain rate at a frequency of 40mm/h. Taken by [16]

3.5 Molecular Absorption in MIMO Capacity

The maximum achievable capacity of a MIMO channel is proportional to the minimum number of the antennas at the receiver and the transmitter. Thus, in an environment that lacks spatial diversity, such capacity would be degraded because of the deficiency of parallel information paths as well as the rank of the MIMO channel between the receiver and the transmitter. Moreover, in a rich scattering environment, scatters provide sufficient NLoS signal components, leading to a better diversity and capacity. Nevertheless, the LoS signal

component will dominate the received signal and thus, would be a decrease of the loss antenna array. In a LoS scenario, for frequencies around 30 GHz to 300 GHz, the maximum MIMO capacity is achievable with some specific array configuration, where the LoS rays are perfectly orthogonal, resulting in an opportunistically full-rank MIMO channel. However, this is not practical for mobile communications, because such kind of optimal antenna setting requires a user steadily holding a device towards a specific direction [3].

The impact of the absorption coefficient in the MIMO capacity and the channel transfer function is calculated for practical purposes in normal air conditions and 60 GHz, while the channel distance is 50 m and the arrays are in parallel formation. According to the foresaid, the value of the absorption coefficient is around 2.7×10^{-2} (figure 3.3). The figure shows that the smaller is absorption coefficient, the larger is the singular value, leading to an ill-conditioned MIMO channel matrix. Nevertheless, the absorption coefficient increases, the singular values are getting closer and the inverse of condition number increases from zero towards one, which implies a higher multiplexing gain. Moreover, by observing the following figure, it can be seen that the 2×2 MIMO capacity doubles that of a SISO channel for a very large absorption coefficient [3].

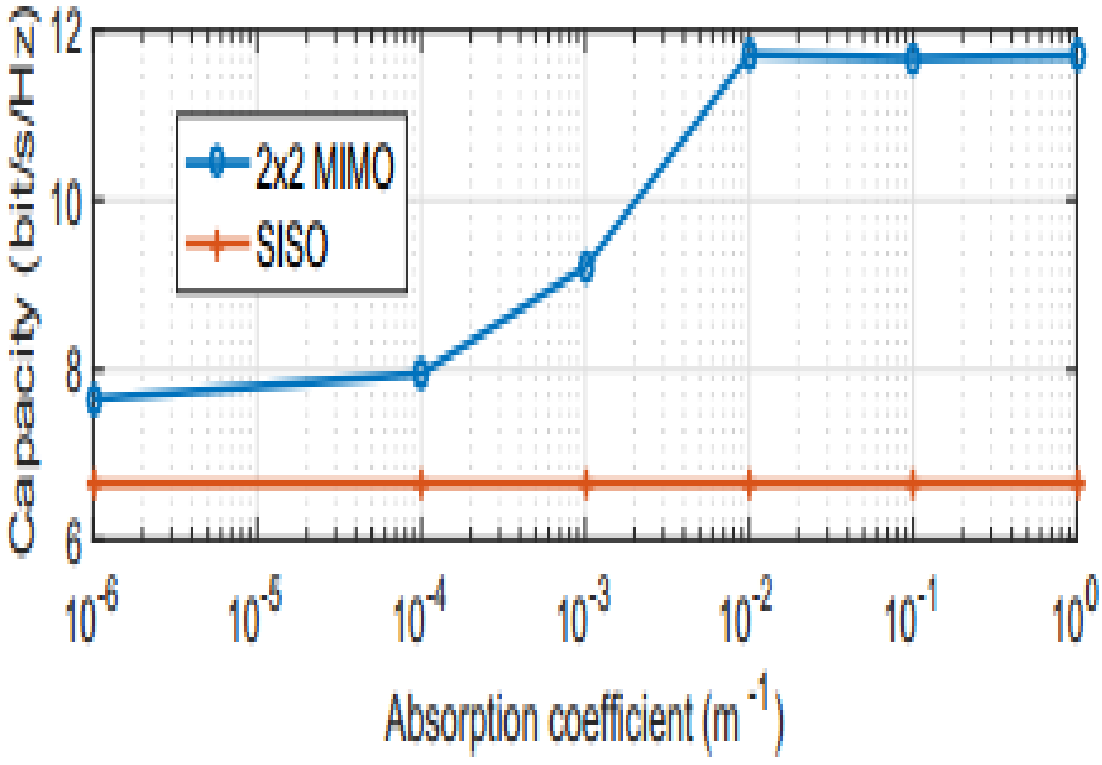

Figure 3.3 Condition number and singular value is affected by molecular absorption. Taken by [3]

3.6 Attenuation, Absorption Coefficient and Re-Radiation in THz

The phenomena of absorption, attenuation and re-radiation are a matter of debate in contemporary research. Research on these subjects have produced various simulation systems which analyze their capacities on the telecommunications [3], [5].

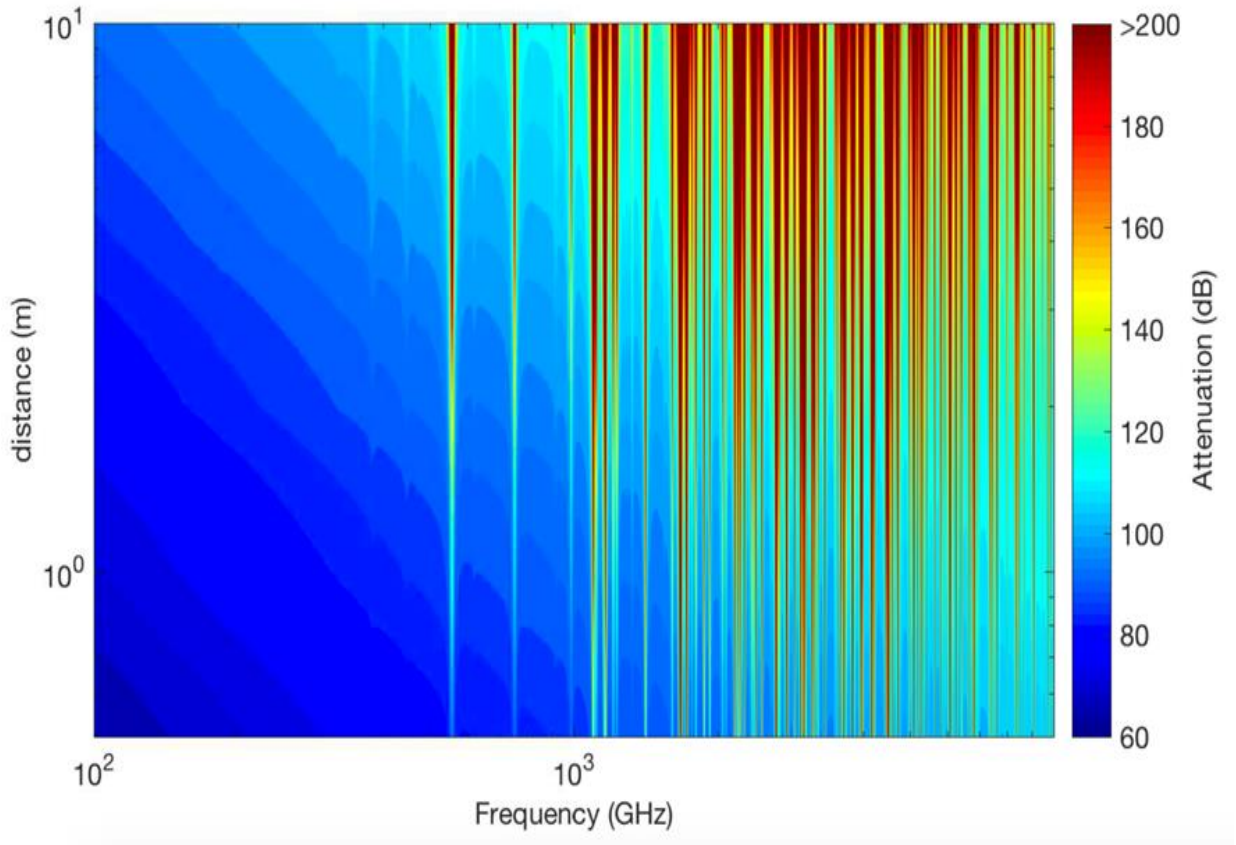

Figure 3.4 Simulation of signal attenuation over distance. Taken by [5]

It has been shown that using random phases on NLoS components, created by molecular re-radiation, allow the examination and evaluation of the MIMO capacity with molecular re-radiation for 5000 times and slow the average result. Moreover, HITRAN's databases are used to generate absorption coefficients for different single gases or some predefined standard gas mixtures at particular atmospheric conditions (i.e. USA model, high latitude, and winter and USA model, tropics), given in Table II. So, the following figure clearly illustrates the corresponding absorption coefficient from 100 GHz to 1000 GHz bands for an ambient temperature of 273 K and standard pressure of 1 atm [3], [5].

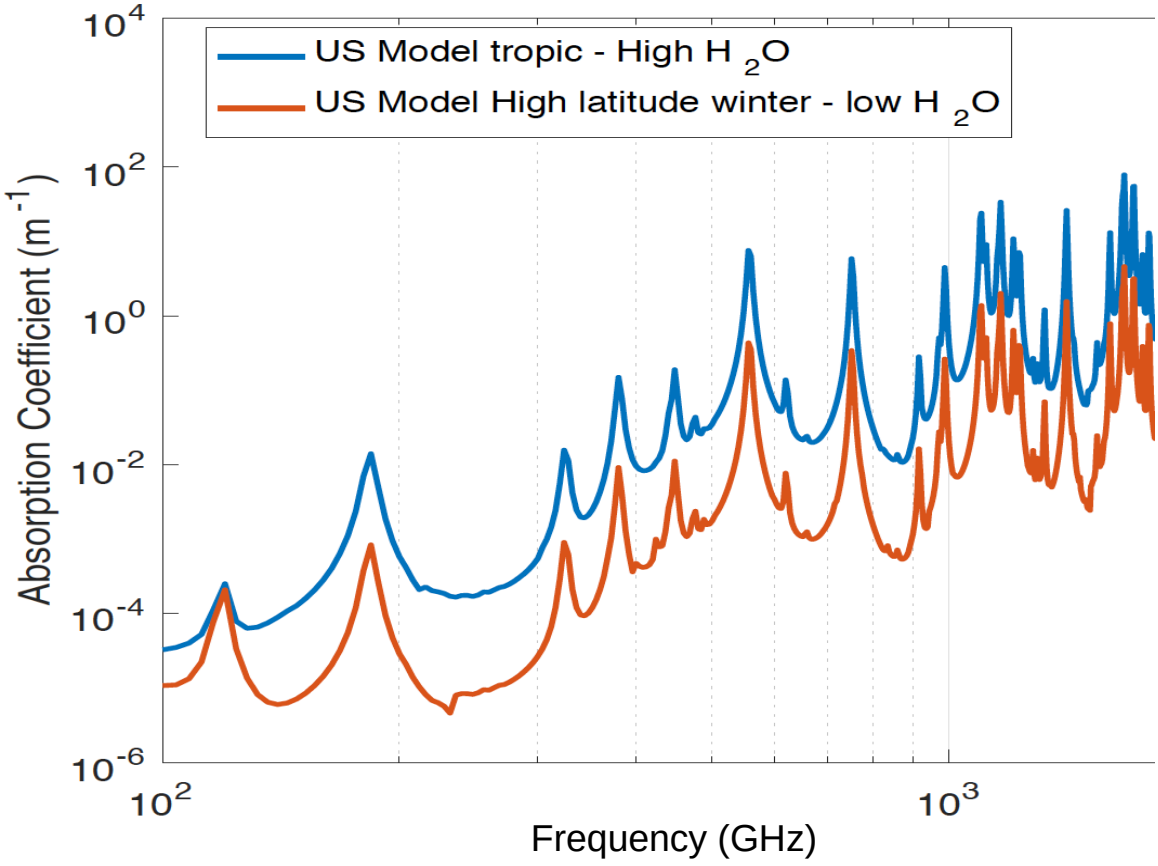

Figure 3.5 Simulation of 225x225 MIMO channel with absorption coefficients in tropic atmosphere. Taken by [5]

It can also be seen from figure 3.5 that there are two major absorption spikes around 100 GHz and 500 GHz. For the former spike, a pair of peaks appear at around 120 GHz, which is attributed to Oxygen molecules. The absorption coefficient is the same for both atmosphere cases: USA model tropic-High H_2O and USA model High latitude winter-Low H_2O, because the percentage of Oxygen is comparable for those two cases. The later spike appears at 180 GHz and is created by water (H_2O) molecules in the air. Thus, in the tropic atmosphere there is a significant increase in terms of the absorption coefficient compare to the win winter atmosphere.

Table I: Simulation parameters [3], [5]

Transmitter and receiver distance (D)	50 m
Inter-element spacing (s)	0.5λ (wave length)
Transmitter arrays angle (ϕ)	90°
Receiver arrays angle (θ)	90°
Number of arrays on each side (n)	3
SNR	20 dB

As it can be observed the maximal values of the signal's attenuation are simulated mostly between 0.1 to 10 meter of distance and around 10^3 to the 10^4 GHz which equals to 1 to 10 THz frequency. What is more, Figure 3.5 shows that for a typical humid or not atmosphere the absorption coefficient has a peak around 6 THz. The absorption coefficient above this frequency is impossible to be estimated due to the signal attenuation and molecular absorption.

The following figures show that the absorption attenuation has a marginal impact on the MIMO capacity improvement as discuss before. As a result, the MIMO system around 100 GHz to 500 GHz can take advantage of the molecular absorption. All the variables were kept constant with the exception of the distance, which value varied to 0.1m, 1m and 10m in each diagram respectively.

Table II: Atmosphere standard gas for different climates. [3], [5]

USA model, mean latitude, summer, H=0	H2O: 1.860000 CO2: 0.033000 O3: 0.000003 N2O: 0.000032 CO: 0.000015 CH4: 0.000170 O2: 20.900001 N2: 77.206000
USA model, mean latitude, winter, H=0	H2O: 0.432000 CO2: 0.033000 O3: 0.000003 N2O: 0.000032 CO: 0.000015 CH4: 0.000170 O2: 20.900001 N2: 78.634779
USA model, high latitude, summer, H=0	H2O: 1.190000 CO2: 0.033000 O3: 0.000002 N2O: 0.000031 CO: 0.000015 CH4: 0.000170 O2: 20.900001 N2: 77.876781
USA model, high latitude, winter, H=0	H2O: 0.141000 CO2: 0.033000 O3: 0.000002 N2O: 0.000032 CO: 0.000015 CH4: 0.000170 O2: 20.900001 N2: 78.925780
USA model, tropics, H=0	H2O: 2.590000 CO2: 0.033000 O3: 0.000003 N2O: 0.000032 CO: 0.000015 CH4: 0.000170 O2: 20.900001 N2: 76.476779

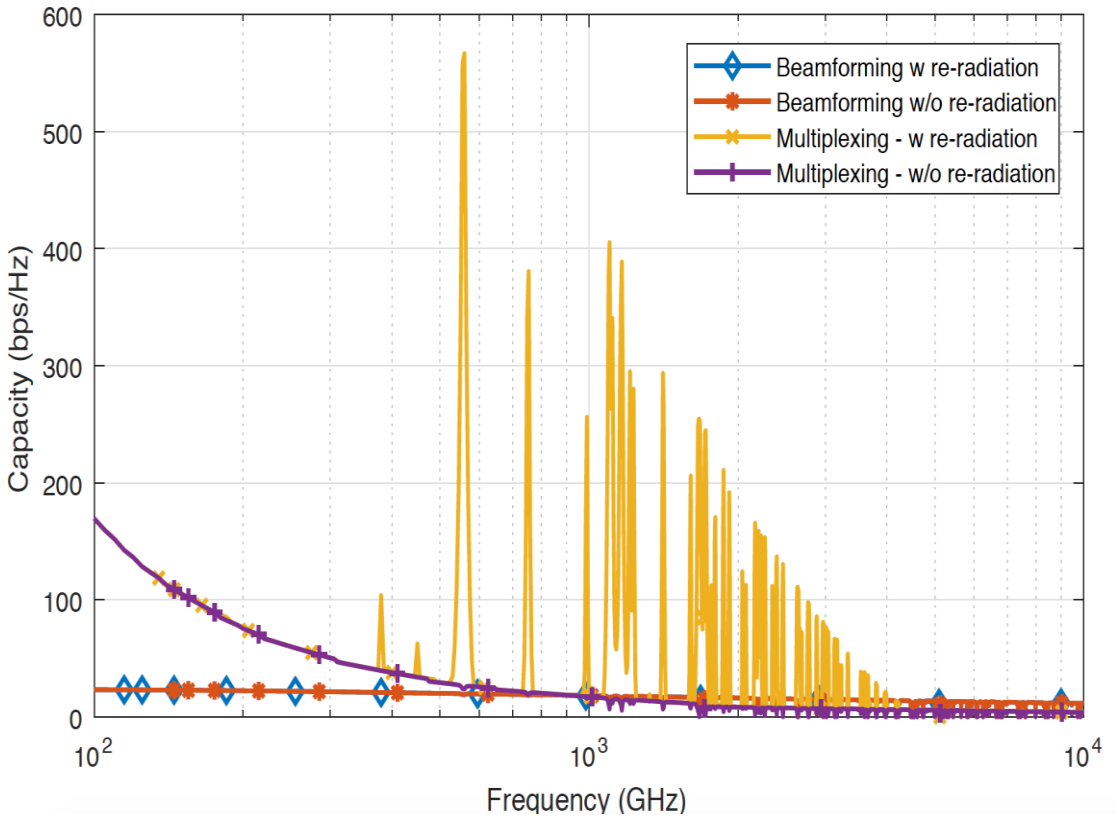

. *Figure 3.6 MIMO channel performance in tropic atmosphere for distance 0.1m and transmitter power 1mW. Taken by* [5]

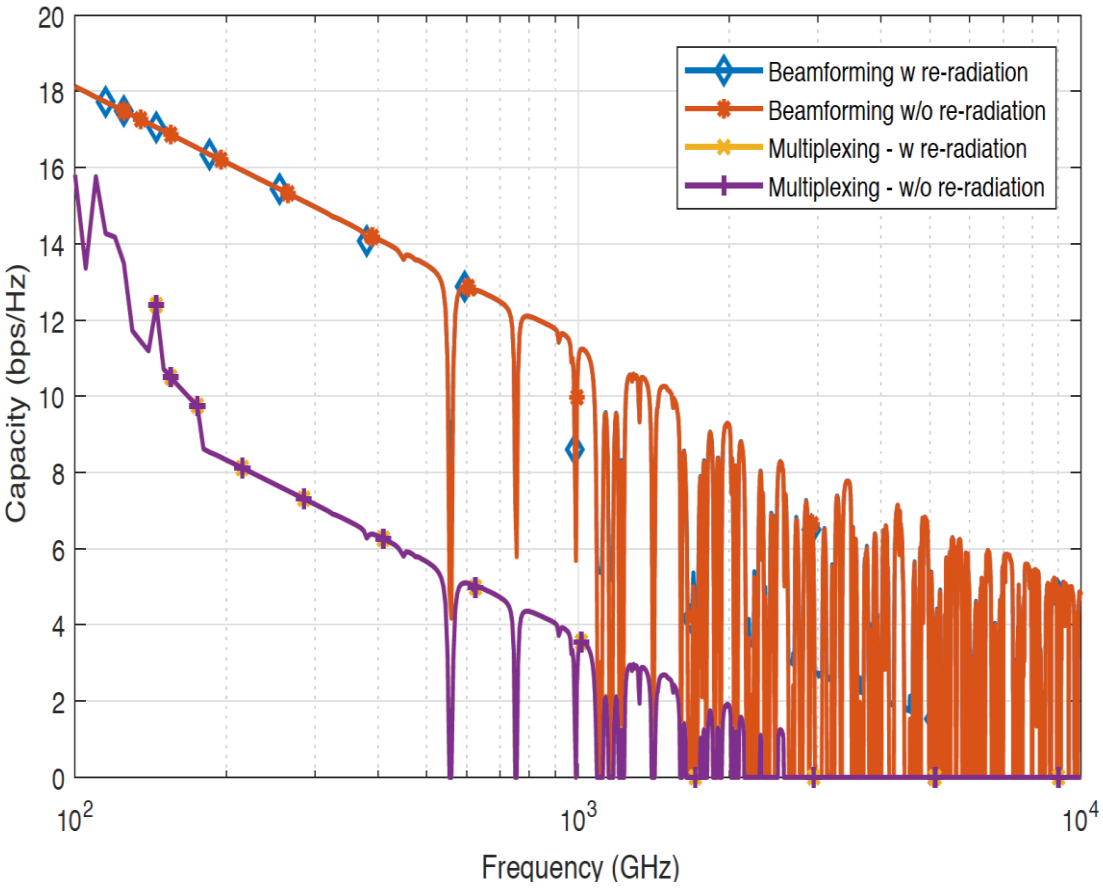

Figure 3.11 MIMO channel performance in tropic atmosphere for distance 1m and transmitter power 1mW. Taken by [5]

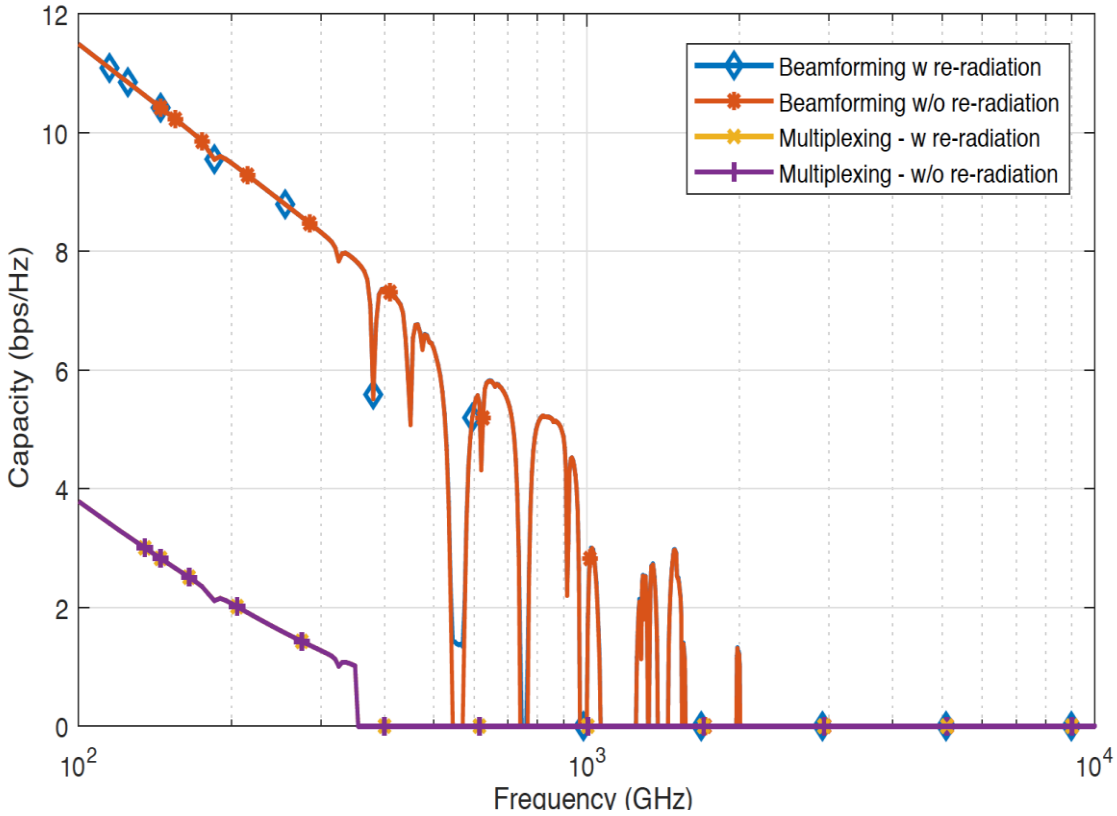

Figure 3.7 MIMO channel performance in tropic atmosphere for distance 10m and transmitter power 1mW. Taken by [5]

Several conclusions can be drawn concerning the above simulations. Firstly, beamforming re-radiation tends to provide higher capacities as distance increases, but lower ones as frequency rises. Secondly, multiplexing re-radiation's capacity has the opposite behavior compare to beamforming re-radiation. Last but not least, on a numerical basis, 0.6 to 0.8 THz frequencies are of a crucial importance for the understanding of THz band behavior as well as for the scientific and commercial progress of the particular band.

Chapter 4

Performance Results from GHz to THz for MIMO Simulation

The main scopes of this thesis are to develop a MIMO experimental simulation, created in a MATLAB environment as well as to deal with the comparison of the MIMO beamforming and multiplexing systems regarding their capacity. The MATLAB code used was the 2017b MATLAB version, with a specific number of samples and with a specific color palette [12].

In order to fulfill the scopes of this thesis two practical approaches were used. In the first attempt the main physical constants and variables were addressed, using some more sophisticated pre-prepared and processed scripts like the K-factor and the absorption coefficient. However, the scripts of the first attempt are where not catalogized as an appendix, but they were essential in order to establish the foundations for the easiest parts of mathematics used. The second attempt is a step-by-step one, creating everything required for the algorithmically experimental simulation. This was also graphically illustrated so as to draw valuable conclusions about the generated surfaces. The variables used were generated by HITRAN. This second attempt has to be noted that it is a more user-friendly approach as it is easy to handle by everyone [17].

Using the absorption coefficient, calculated in the first attempt, the power allocation schemes as well as atmospheric conditions from Table II and assuming that the transmission bandwidth is 50 GHz and the central frequencies are from 300 GHz to 500 GHz, the effectiveness of the THz link in terms of capacity was quantitatively compared. As far as the transmission distance is concerned, path lengths ranging from 0.1 to 10 m were utilized. Furthermore, it is important to note that the following figures derived by using the equations from the Chapter 2 and 3.

Last but not least, the effectiveness of the THz system is evaluated, revealing that the frequency selectivity of the THz channel increases, as the range of the wireless link increases. THz link performance is also found to be depended on the atmospheric conditions.

4.1 Absorption Coefficient

```
% attenuation due to absorption script

% HITRAN 7 may be not precise
% use of own values of molecular absorption coefficient k

function [abs_c] = absorption_coefficient(f,model,T,P)

% Function to calculate the total absorption coefficient from a
prescribed
% set of atmospheric conditions and given frequency.

% f = frequency [THz]

% model = atmospheric model (of H2O, CO2, O3, N2O, CO, CH4, O2,
N2) from
% HITRAN database
%   1: mean latitude, summer
%   2: mean latitude, winter
%   3: high latitude, summer
%   4: high latitude, winter
%   5: tropical

% T = (system) temperature [oC], we need [K] so ...+273.15

% P = (system) pressure [atm]

% Given constant parameters:
T_STP = 273.15; % Standard temperature [K]

P_STP = 1; % Standard pressure [atm]

N_A = 6.0221*10^23; % Avogadro constant [molecules/mol]

R = 8.2051*10^(-5); % Gas constant [m3 atm/molK]

c = 2.9979*10^8; % Light speed [m/s]

kB = 1.3806*10^(-23); % Boltzmann constant [J/K]

h = 6.6262*10^(-34); % Planck constant [Js]

load weather; % weather carries the atmospheric model

load lineintensity; % carries the values of spectral line inten-
sity
load a0air;

load a0; %is lorez half width [11]

Weather = table2array(weather);
load mfcp0; % mfcp0 = the same for zero pressure

load delta; %linear pressure shift

f = f.*10^(12);
```

```
mfc = mfcp0.*c.*10^10 + 10^10.*delta.*(P/P_STP); % mfc = mean
resonance frequency

abs_c = 0; % initialize sum

for j=1:width(weather)
    aL(j)       =       ((1-                              Weath-
er(model,j)).*a0air+Weather(model,j).*a0).*(P./P_STP).*(T_STP./(T
+273.15)).^0.5; % Lorentz half-width
    abs_c                =                abs_c                +
((T_STP.*N_A)/(P_STP.*R))*(P./(T+273.15))^2.*Weather(model,j).*li
neintensity(j).*(aL(j)./pi).*((1./(aL(j).^2+(f-
mfc).^2))+1./(aL(j).^2+(f+mfc).^2)).*(f/mfc).^2.*c.*tanh(h.*c.*f.
/(2.*kB.*(T+273.15))./tanh(h.*c.*mfc./(2.*kB.*(T+273.15)));

end

endlength(dist);
b1 = length(k_new);

for a = 1:a1

     for b = 1:b1

     a_abs(b,a) = exp(dist(a).*(-k_new(b)));

     end

end
disp("The attenuation absorption has been estimated as a matrix
of molecular absorption coefficients and distance.")
```

The MATLAB script presented above is coding the attenuation absorption correlation, deriving from the equations (3.7) and (3.8). Where f is the frequency which can be any value mostly from 300 GHz to 500GHz, with bandwidth 50 GHz, T is system temperature which varies from 0^oC to 50^oC (for Kelvin scale from is 273.15 K to 323.15 K), P is system pressure which varies 1 atm to 2 atm, T_{stp} is the standard temperature 273.15 K, P_{stp} is the standard pressure 1 atm, N_A is Avogadro constant 6.0221×10^{23}, R is Gas constant 8.2051×10^{-5}, c is the light speed 2.9979×10^{8}, k_B is the Boltzmann constant 1.3806×10^{-23}, h is the Planck constant 6.6262×10^{-34} , a_L is lorez half-width from database and q is the weather carries the atmospheric model from Table II and δ is 0.5 [11].

The absorption coefficient vector for varying values of frequency, temperature and pressure for any of the five atmospheric models mentioned in Table II are calculated. Specifically, for frequency 500 GHz, temperature 25^oC and pressure 1 atm the absorption coefficient vector is:

$$\overrightarrow{A_{abs}(f)} = 10^{-4}(0.2166,0.0152,00929,0.0030,0.4103)$$

Similarly, for frequency 300 GHz, temperature $25^{o}\mathrm{C}$ and pressure 1 atm the absorption coefficient vector is:

$$\overrightarrow{A_{abs}(f)} = 10^{-4}(0.2196, 0.0154,0.0942,0.0030,0.4159)$$

Furthermore, for frequency 500 GHz, temperature $40^{o}\mathrm{C}$ and pressure 1.015 atm, the condition of a valley on a very hot day, the absorption coefficient vector is:

$$\overrightarrow{A_{abs}(f)} = 10^{-4}(0.1945,0.0137,0.0834,0.0027,0.3684)$$

Finally, for frequency 1.25 THz, temperature $5^{o}\mathrm{C}$ and pressure 1 atm, a point with a very high latitude and very cold weather which is an extreme example, the absorption coefficient vector is:

$$\overrightarrow{A_{abs}(f)} = 10^{-4}(0.2560,0.0137,0.0834,0.0027,0.4849)$$

The best atmospheric model out of the five presented in Table II is the one having the smallest value of absorption. For example, for $\overrightarrow{A_{abs}(f)} = 10^{-4}$ is the high latitude for summer with a value of absorption of only 0.0027.

4.2 K-factor Surface Plot

Having estimated the absorption coefficient, the K-factor is calculated by using the equation (3.1) where d is the pre-determined space distance from 0.1 to 10 m.

```
% K-factor plotting

clear
clc

load distance;

% Press frequency in THz, temperature in oC and pressure in atm

f = 0.001; % f = frequency [THz]

T = 20; % T = temperature [oC]

P = 1; % P = pressure [atm]

ABS_C = ABSORPTION_COEFFICIENT_VECTOR(f,T,P)';

minABS_C = min(ABS_C);

maxABS_C = max(ABS_C);
```

```
distance = distance';

k = (maxABS_C-minABS_C)/(length(distance)-1);

ABS_C = minABS_C:k:maxABS_C;

for a = 1:length(distance)
    for b = 1:length(ABS_C)
        K_factor(b,a)     =     exp(distance(a).*(-ABS_C(b)))./(1-
exp(distance(a).*(-ABS_C(b))));
    end
end

con-
tourf(log10(ABS_C),log10(distance),10*log10(K_factor),'linestyle'
,'none','DisplayName','K-factor (dB)') % K_factor in dB

title(['K-factor for f=',num2str(f),'THz.']);
xlabel('Absorption Coefficient (m^{-1})');
ylabel('Distance (m)')
colorbar;

legend('show')
```

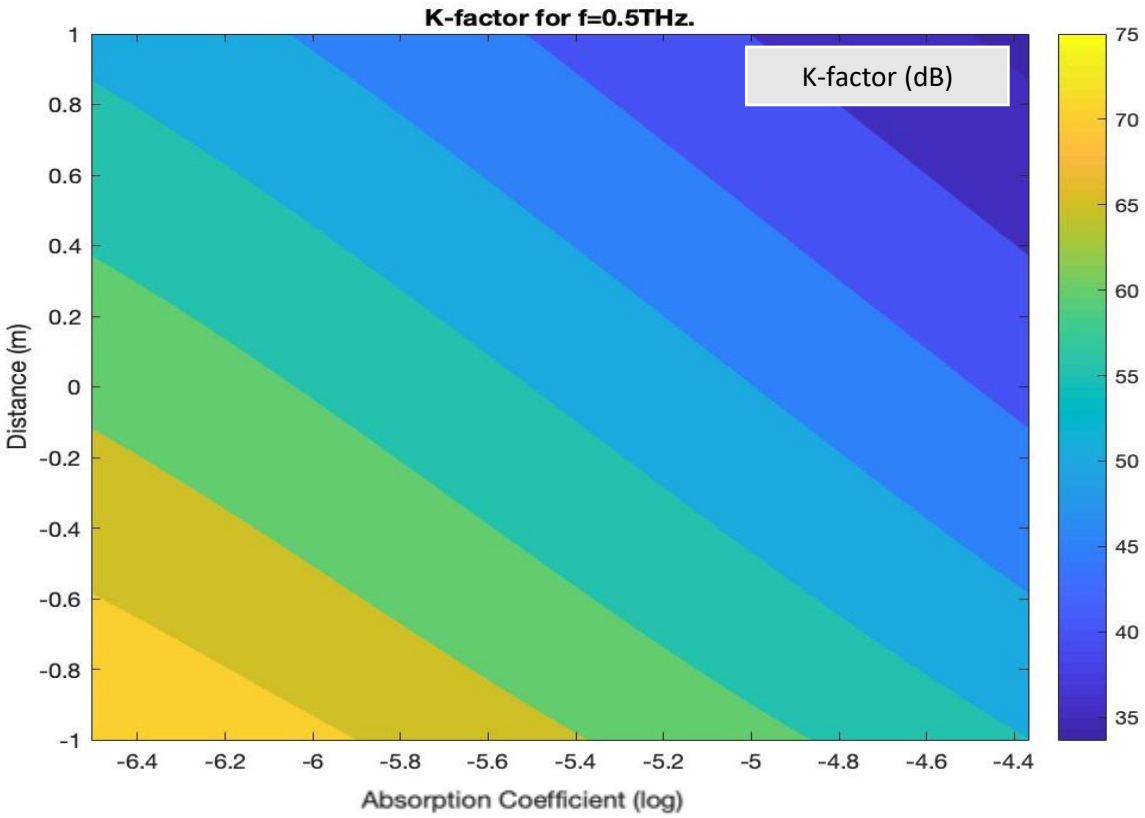

Figure 4. 1 The K-factor plot with frequency 500 GHz shows the relationship of the pre-determined space distance between 0.1 to 10 meter and the absorption coefficient for standards atmospheric models from Table II.

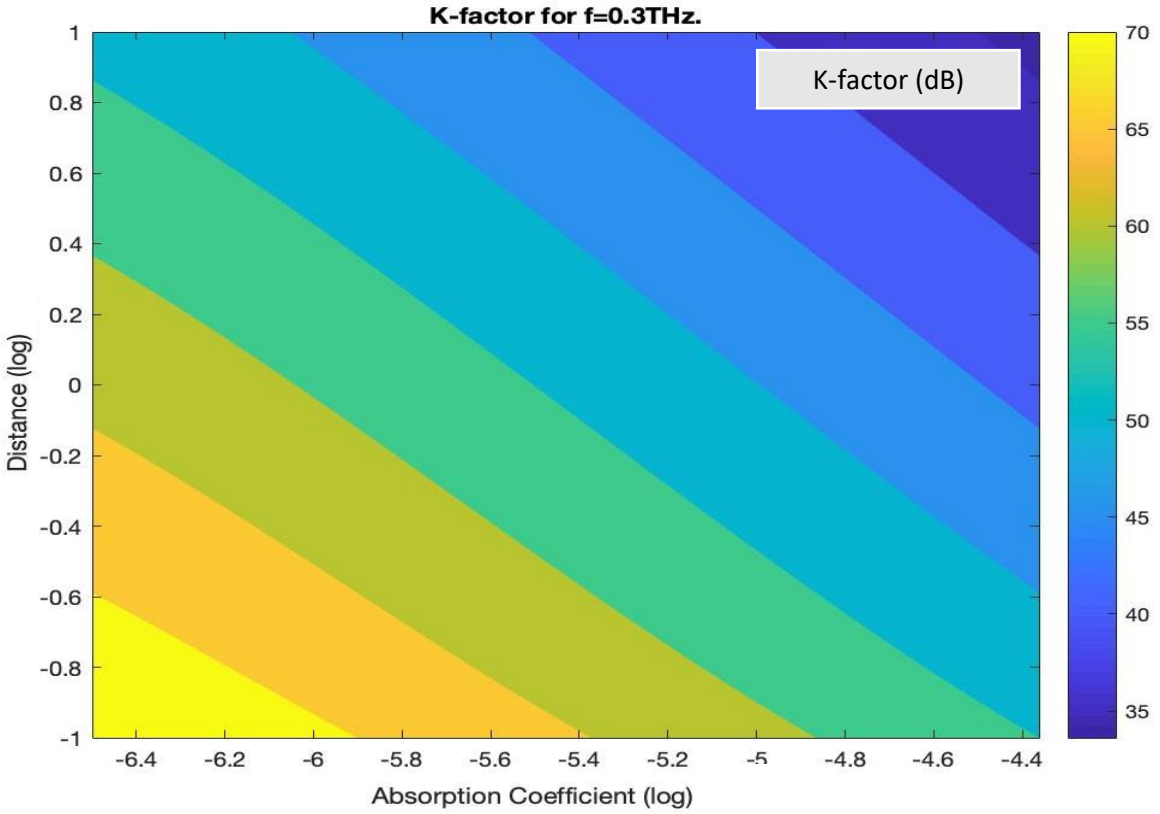

Figure 4.2 The K-factor plot with frequency 300 GHz shows the relationship of the pre-determined space distance between 0.1 to 10 meter and the absorption coefficient for standards atmospheric models from Table II.

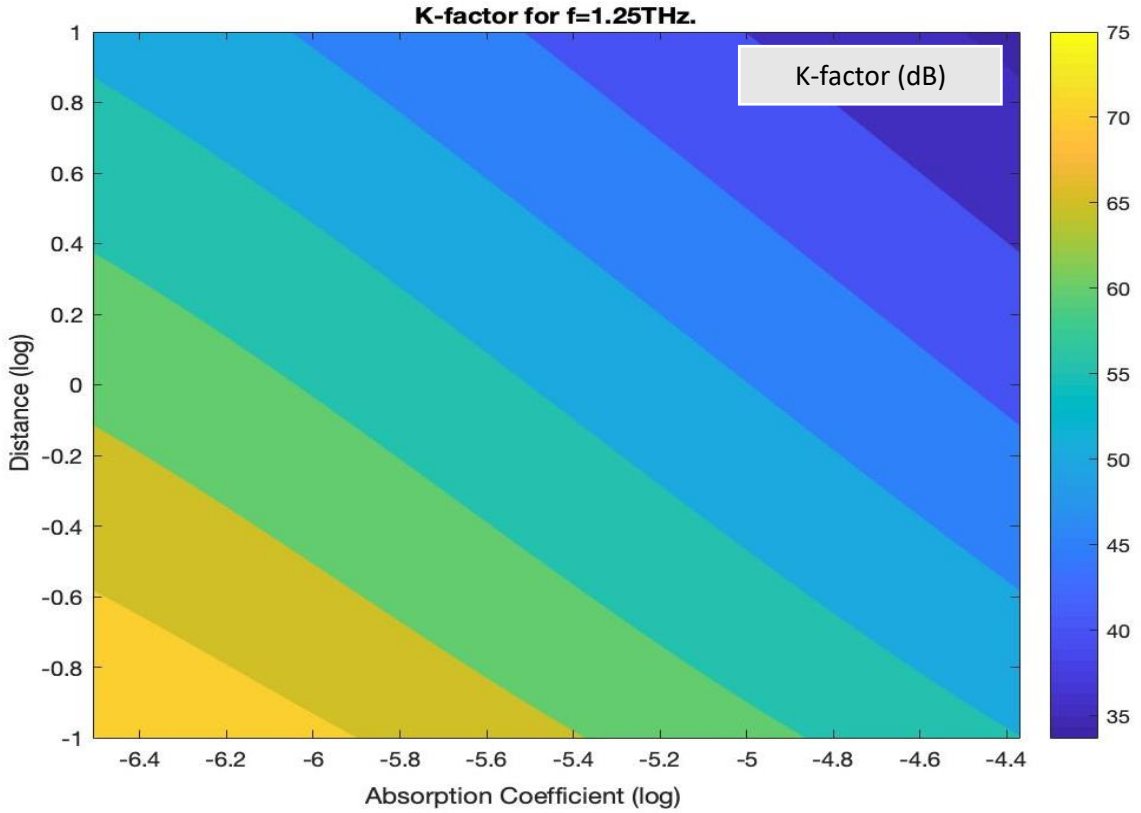

Figure 4.3 The K-factor plot with frequency 1250 GHz shows the relationship of the pre-determined space distance between 0.1 to 10 meter and the absorption coefficient for standards atmospheric models from Table II.

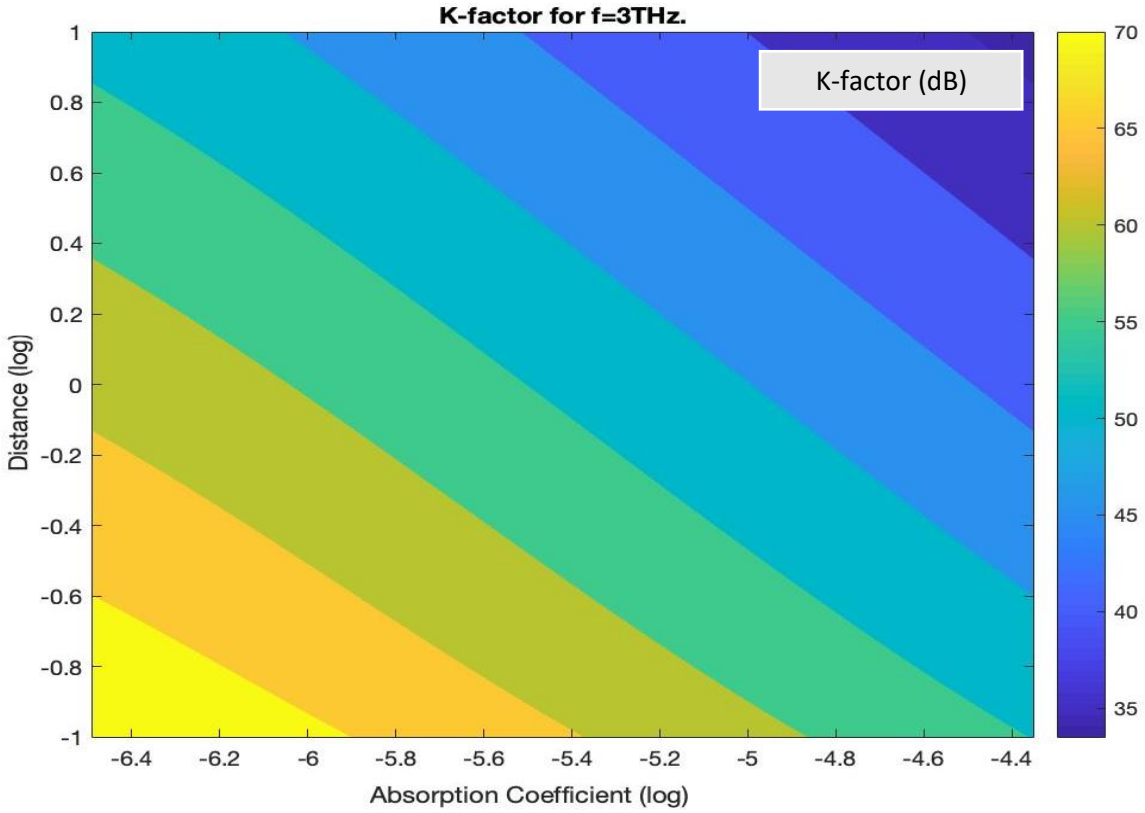

Figure 4.4 The K-factor plot with frequency 3000 GHz shows the relationship of the pre-determined space distance between 0.1 to 10 meter and the absorption coefficient for standards atmospheric models from Table II.

The figures illustrate the K-factor in relation to the distance and the absorption coefficient. Where f is the frequency which can vary from 275 GHz and 550 THz, with bandwidth 15-20 GHz, T is the system temperature which can take values from $0^o\mathrm{C}$ to $50^o\mathrm{C}$, and P is the system pressure which can take values from 1 atm to 1.05 atm. Each figure was produced for specific values of frequency, temperature and pressure.

In particular, figure 4.1 was developed for frequency 500 GHz, temperature $25^o\mathrm{C}$ and pressure 1 atm. It can be seen that for absorption coefficient $10^{-5.4}$ and distance 1 m the K-factor is 56.5 dB. Similarly, figure 4.2 was produced for frequency 300 GHz, temperature $25^o\mathrm{C}$ and pressure 1 atm. For the same values of the absorption coefficient and distance the K-factor is 52.5 dB. Moreover, figure 4.3 was developed for frequency 1250 GHz, temperature $20^o\mathrm{C}$ and pressure 1 atm. In this case, for absorption coefficient $10^{-5.4}$ and distance 1 m the K-factor is 51 dB. Finally, figure 4.4 was plotted for frequency 3000 GHz, temperature $14.7^o\mathrm{C}$ (the average earth temperature) and pressure 1 atm. So, for absorption coefficient $10^{-5.4}$ and distance 1 m, the K-factor is 54 dB.

It is revealed that although the maximum theoretical value of the K-factor is 75 dB, in figures 4.1 and 4.3 it is invisible. On the contrary, the maximum value of the K-factor is visible in figures 4.2 and 4.4. What is more, in all cases there is a small increase of K-factor for low values of distance and absorption coefficient. Moreover, it is evident that for a fixed transmission frequency, there is a slight increase of the K-factor regarding the values of distance and absorption coefficient. On the other hand, figures 4.2 and 4.4 show that although the maximum value for K-factor is 70 dB, there is a higher rate of increase of K-factor. Last but not least, it should be mentioned that all figures are shown to follow the pure loss channel mode of Hosseini's theoretical K-factor plot [5].

4.3 MIMO Capacity in High Frequencies

Using the equations 2.13 and 2.15 and the Hosseini's model a variety of multiplexing and beamforming capacities are calculated.

```
% Capacity script:
% Hoseini et al. beamforming and multiplexing MIMO capacities.

clear

clc


c = 2.9979*10^8; % Light speed [m/s]

load distance;

n_t = 25; % n_t = transmitting antennas

n_r = 25; % n_r = receiving antennas

f = 0.5; % f = frequency [THz]

T = 25; % T = temperature [oC]

P = 1; % P = pressure [atm]

model = 1; % atmospheric model [1...5]

PR = 10; % transmission power [mW]

% sigma squared = 1

% Signal-to-Noise Ratio [dB] from transmission power

% ABS_C = ABSORPTION_COEFFICIENT_VECTOR(f,T,P)';
```

```
% minABS_C = min(ABS_C);

% maxABS_C = max(ABS_C);

% k = (maxABS_C-minABS_C)/(length(distance)-1);

% ABS_C = minABS_C:k:maxABS_C;

% distance = distance';

K = absorption_coefficient(f,model,T,P);

for i = 1:n_r
    for j = 1:n_t
        dist(i,j)    =    min(distance)+rand(1,1).*(max(distance)-
min(distance)); % random generation of d_ij's
        h(i,j)         =         (c./(4*pi.*f.*dist(i,j))).*(exp(-
K.*dist(i,j)./2+2.*pi.*1i.*dist(i,j)./c)+sqrt(1-exp((-
K.*dist(i,j))).*exp(2.*1i.*pi.*beta(1,1))));
        % h_i,j channel transfer functions, h channel matrix,
where the
        % antennas are randomly placed in the simulation space
    end
end

H = h*conj(h);

E = eig(H); % the eigenvalue column vector of H

tr = trace(H);

max_MIMO_beamforming_Capacity      =      real(log10(1+(PR.*10^(-
3)).*tr)); % bps - we transfer all power from the trace of
% the eigenvalues to one antenna set

MIMO_beamforming_Capacity        =        real(log10(1+(PR.*10^(-
3)).*max(E))); % bps - we transfer all power from the maximum
% eigenvalue to one antenna set

MIMO_spatial_multiplexing_Capacity              =              re-
al(sum(log10(1+(PR.*0.001/min(n_t,n_r)).*E))); % bps

%MIMO_spatial_multiplexing_Capacity_1 = 0;
%for i=1:length(E)
%                       MIMO_spatial_multiplexing_Capacity_1      =
MIMO_spatial_multiplexing_Capacity_1                              +
log10(1+(PR.*0.001).*E(i));
%end
```

The MATLAB script presented above is coding the theoretical maximum MIMO beamforming capacity (depending on the trace of the table), the MIMO beamforming capacity and the MIMO spatial multiplexing capacity as function of the equations 2.13 and 2.15. Where f is the frequency with values mostly from 300 GHz to 500GHz, bandwidth around 50 GHz, T is the system temperature

ranging between 0^oC to 50^oC, P is the system pressure from 1 atm to 2 atm, distance is the pre-determined space distance ranging between 0.1 to 10 meters, c is light speed 2.9979×10^8, n_t and n_r are the numbers of transmitting and receiving antennas respectively (the product of which $n_t \times n_r$ results possible different randomly distances), “model” is the weather carries the atmospheric model from Table II, PR is the transmission power in mW (i.e. the signal to noise ratio) and sigma squared is 1.

The maximum MIMO beamforming capacity, the MIMO beamforming capacity and the MIMO spatial multiplexing capacity for varying values of frequency, temperature and pressure for any of the five atmospheric models mentioned in Table II are calculated. However, the first atmospheric model is mostly used due to the fact that gives the average moisture content in the atmosphere.

In particular, for frequency 500 GHz, temperature 25^oC, pressure 1 atm, for first atmospheric model, for number of antennas $n_t = n_r = 225$, for PR transmission power 1 mW and for average random distance from the “load distance” table (i.e. capacities are ergodic quantities) the values of each of the MIMO capacities are:

$$C_{Beamforming}^{max} = 14.3956\ Gbps$$

$$C_{Beamforming} = 14.3833\ Gbps$$

$$C_{Spacial\ Multiplexing} = 283.5215\ Gbps$$

Similarly, for frequency 500 GHz, temperature 25^oC, pressure 1 atm, for first atmospheric model, for number of antennas $n_t = n_r = 225$, for PR transmission power 10 mW and for average random distance from the “load distance” table the values of each of the MIMO capacities are:

$$C_{Beamforming}^{max} = 17.4343\ Gbps$$

$$C_{Beamforming} = 17.4083\ Gbps$$

$$C_{Spacial\ Multiplexing} = 2{,}879.6001\ Gbps$$

The second example reveals that the special multiplexing capacity is very high, and this is in scientific agreement with the Hosseini third plot. Nonetheless, this is observed only in the extreme value of 10 mW [5].

4.4 Comparison and Plotting MIMO Capacity in THz

The MIMO beamforming and multiplexing capacity for both Hosseini and Simplified model is presented in the following MATLAB script. The Simplified model is produced by using the equations 3.10, 3.11, 3.12, 3.13, 3.14, 3.15, 3.16, 3.17, 3.18 and 3.19. The main difference between the two models is that Hosseini's uses the atmospheric models from HITRAN, while the Simplified model is more flexible with water evaporation.

```
% Capacity plot script
% 1) Hoseini et al. beamforming and spatial multiplexing
% 2) Kookoniemi et al. -//-.
clear
clc
% 1)plot
c = 2.9979*10^8; % Light speed [m/s]
load distance;
n_t = 10; % n_t = transmitting antennas
n_r = 10; % n_r = receiving antennas
f = 0.275; % f = frequency [THz]
T = 25; % T = temperature [oC]
P = 1; % P = pressure [atm]
model = 1; % atmospheric model [1...5]
PR = 10; % transmission power [mW]
% sigma squared = 1
% Signal-to-Noise Ratio [dB] from transmission power
l = (max(distance)-min(distance))./(100*n_r-1);
Dist = min(distance):l:max(distance);
ABS_C = ABSORPTION_COEFFICIENT_VECTOR_atm(f,T,P);
minABS_C = min(ABS_C);
maxABS_C = 10^(7)*max(ABS_C);
```

```
k = (maxABS_C-minABS_C)/(100*n_t-1);

ABS_C = minABS_C:k:maxABS_C;

% K = absorption_coefficient(f,model,T,P);

for i = 1:100*n_r
    for j = 1:100*n_t
        %if i <= floor(n_r./3)
        %    Dist(i) = 0.1; %  generation of d_ij's
        %elseif i <= floor(2*n_r/3)
        %    Dist(i) = 1; %  generation of d_ij's
        %else
        %    Dist(i) = 10;
        %end
        h(i,j) = (c./(4*pi.*f.*Dist(i))).*(exp(-
ABS_C(j).*Dist(i)./2+2.*pi.*1i.*Dist(i)./c)+sqrt(1-exp((-
ABS_C(j).*Dist(i))).*exp(2.*1i.*pi.*beta(1,1))));
        % h_i,j channel transfer functions, h channel matrix,
where the
        % antennas are randomly placed in the simulation space
    end
end

H = h*conj(h);
E = eig(H); % the eigenvalue column vector of H
tr = trace(H); % the trace of H (sum of principal diagonal = sum
of eigenvalues)

for i = 1:100*n_r
    for j = 1:100*n_t
        MIMO_Beamforming_Capacity(i,j) =  re-
al(log10(1+(PR*0.001).*(H(i,j))));
        MIMO_Spatial_Multiplexing_Capacity(i,j) =
n_t*real(log10(1+(PR*0.001/min(n_r,n_t)).*H(i,j)));
    end
end

%MIMO_beamforming_Capacity = real(log10(1+(PR.*10^(-3)).*tr)); %
bps - we transfer all power from the trace of
% the eigenvalues to one antenna set

%MIMO_spatial_multiplexing_Capacity = re-
al(sum(log10(1+(PR.*0.001).*E))); % bps

% 2)plot

phi = 1.86;

ABS_C_simple = absorption_loss(f,T,P,phi);

ABS_C_simple = 10^(-5)*ABS_C_simple;

% n = (max(ABS_C_simple)-min(ABS_C_simple))/(length(distance)-1);

% ABS_C_SIMPLE = min(ABS_C):n:max(ABS_C);

m = (max(distance)-min(distance))/(length(distance)-1);
```

```
DIST = min(distance):m:max(distance);

for i = 1:length(DIST)
    for j = 1:length(ABS_C_simple)
        h1(i,j) = (c./(4*pi.*f.*DIST(i))).*(exp(-
ABS_C_simple(j).*DIST(i)./2+2.*pi.*1i.*DIST(i)./c)+sqrt(1-exp((-
ABS_C_simple(j).*DIST(i))).*exp(2.*1i.*pi.*beta(1,1))));
        % h_i,j channel transfer functions, h channel matrix,
where the
        % antennas are randomly placed in the simulation space
    end
end

H1 = h1*conj(h1);
E1 = eig(H1); % the eigenvalue column vector of H
tr1 = trace(H1); % the trace of H (sum of principal diagonal =
sum of eigenvalues)

for i = 1:length(DIST)
    for j = 1:length(ABS_C_simple)
        MIMO_Beamforming_Capacity_Simplified_model(i,j) =  re-
al(log10(1+(PR*0.001).*(H1(i,j))));
        MIMO_Spatial_Multiplexing_Capacity_Simplified_model(i,j)
=  n_t*real(log10(1+(PR*0.001/min(n_r,n_t)).*H1(i,j)));
    end
end

% 3)plot

Dist = Dist';

subplot(2,2,1);
con-
tourf(log10(ABS_C),log10(Dist),MIMO_Beamforming_Capacity,'linesty
le','none','DisplayName','Capacity (bps)') % K_factor in dB
title(['MIMO Beamforming Capacity for f=',num2str(f),'THz.']);
xlabel('Absorption Coefficient (log) (m^{-1})');
ylabel('Distance (log) (m)')
colorbar;
colormap(jet)
legend('show')

subplot(2,2,2);
con-
tourf(log10(ABS_C),log10(Dist),MIMO_Spatial_Multiplexing_Capacity
,'linestyle','none','DisplayName','Capacity (bps)') % K_factor in
dB
title(['MIMO Spatial Multiplexing Capacity for
f=',num2str(f),'THz.']);
xlabel('Absorption Coefficient (log) (m^{-1})');
ylabel('Distance (log) (m)')
colorbar;
legend('show')

subplot(2,2,3);
con-
tourf(log10(ABS_C_simple),log10(distance),MIMO_Beamforming_Capaci
```

```
ty_Simplified_model,'linestyle','none','DisplayName','Capacity
(bps)') % K_factor in dB
title(['Simplified model MIMO Beamforming Capacity for
f=',num2str(f),'THz.']);
xlabel('Absorption Coefficient (log) (m^{-1})');
ylabel('Distance (log) (m)')
colorbar;
colormap(jet)
legend('show')

subplot(2,2,4);
con-
tourf(log(ABS_C_simple),log10(distance),MIMO_Spatial_Multiplexing
_Capacity_Simplified_model,'linestyle','none','DisplayName','Capa
city (bps)') % K_factor in dB
title(['Simplified model MIMO Spatial Multiplexing Capacity for
f=',num2str(f),'THz.']);
xlabel('Absorption Coefficient (log) (m^{-1})');
ylabel('Distance (log) (m)')
colorbar;
legend('show')
```

The Hosseini's model is the first part of the code (plot 1). Where f is the frequency with values mostly from 275 GHz to 500GHz, bandwidth ranging between 30 to 50 GHz, T is the system temperature ranging between $0^o\mathrm{C}$ to $50^o\mathrm{C}$, P is the system pressure between 1 atm to 2 atm, distance is the pre-determined space distance between 0.1 to 10 meters (the average random distance from the "load distance" table is used), c is light speed 2.9979×10^8, n_t and n_r are the numbers of transmitting and receiving antennas respectively, "model" is the weather carries the atmospheric model from Table II, the first atmospheric model is mostly used due to the fact that gives the average moisture content in the atmosphere, PR is the transmission power in mW (i.e. the signal to noise ratio) and sigma squared is 1. Using the equations 2.13 and 2.15, initially the absorption coefficient vector and the K-factor are calculated, keeping the values of frequency, temperature and pressure constant and equal with those given at the first atmospheric model. Then, the MIMO capacities for Hosseini's model are estimated.

Furthermore, the Simplified model is utilized to calculate the relative humidity and then, the absorption coefficient (equation 3.12), using the same parameter values as the ones used in Hosseini's model. In an effort to compare the two model's *phi* is taken equal to 1.86 as this is the closest value in the first atmospheric model (Table II) for water vapor $H_2O = 186000$. Consequently, the absorption coefficient

and the K-factor for the Simplified model are estimated, followed by the beamforming and multiplexing capacities, using the equations 2.13 and 2.15.

Finally, the plots for the beamforming and special multiplexing for both Hosseini and Simplified models are produced, applying the MATLAB script. Although the figures 4.5, 4.6, 4.7, 4.8 as well as the figures 4.9, 4.10, 4.11, 4.12 and the figures 4.13, 4.14, 4.15, 4.16 are actually one image, the images were fragmented in order to observe the results more clearly.

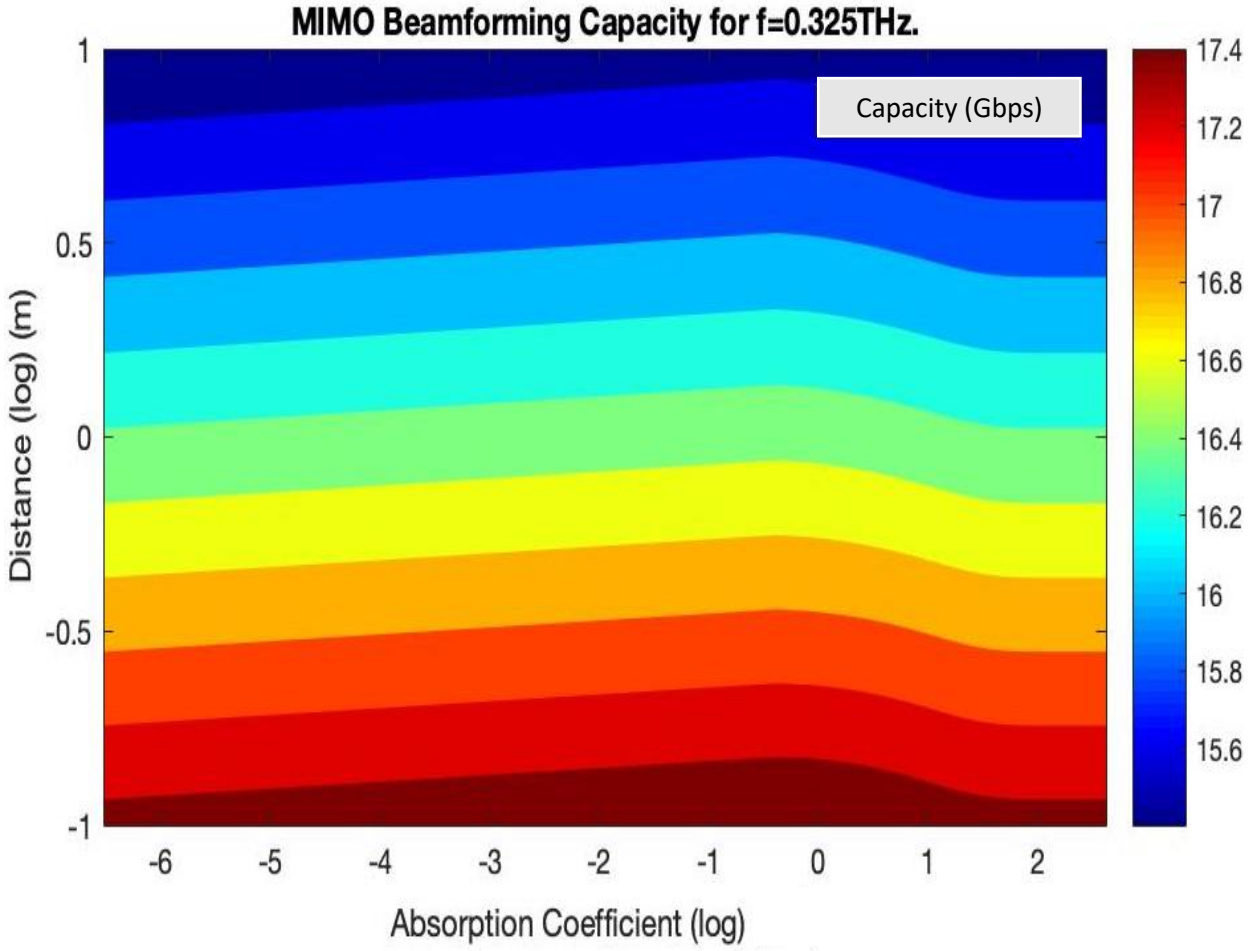

Figure 4.5 MIMO beamforming capacities plot with frequency 325 GHz which shows the relationship between the pre-determined space distance, ranging from 0.1 to 10 meters, and the absorption coefficient, according to Hosseini's model.

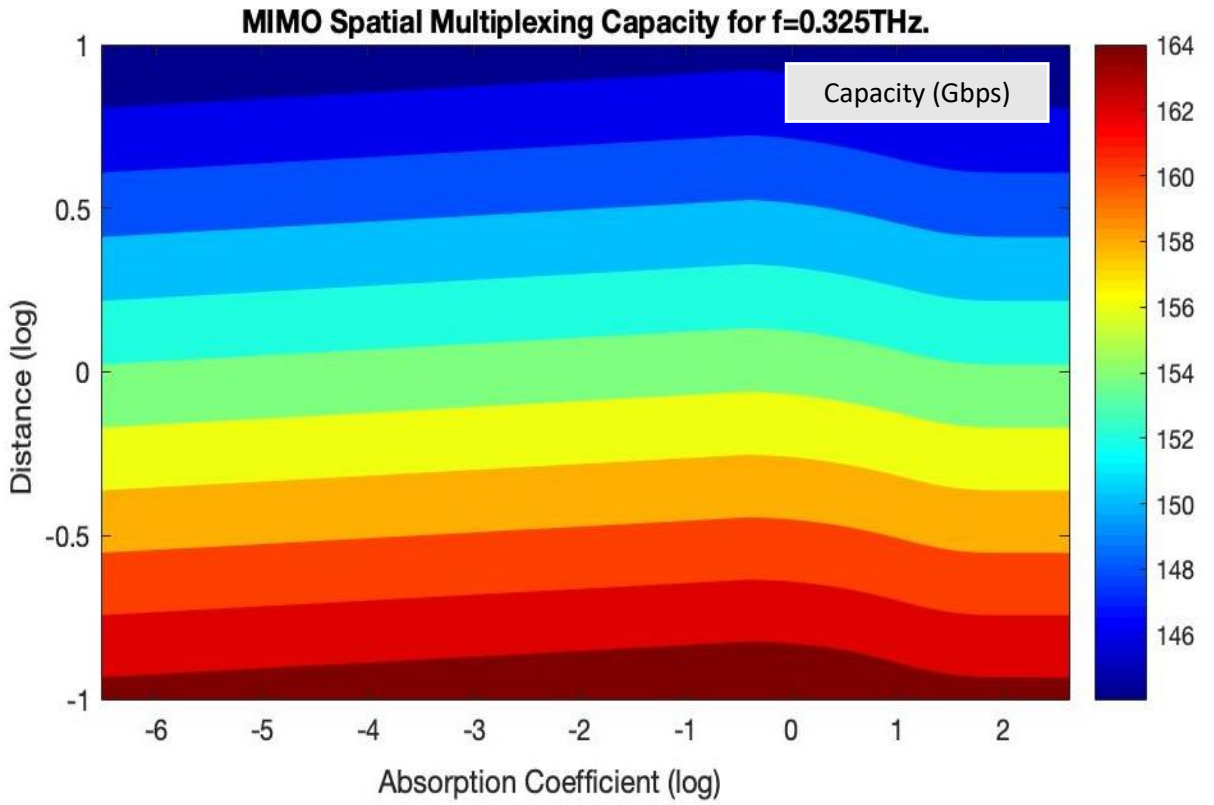

Figure 4.6 MIMO special multiplexing capacities plot with frequency 325 GHz which shows the relationship between the pre-determined space distance, ranging from 0.1 to 10 meters, and the absorption coefficient, according to Hosseini's model.

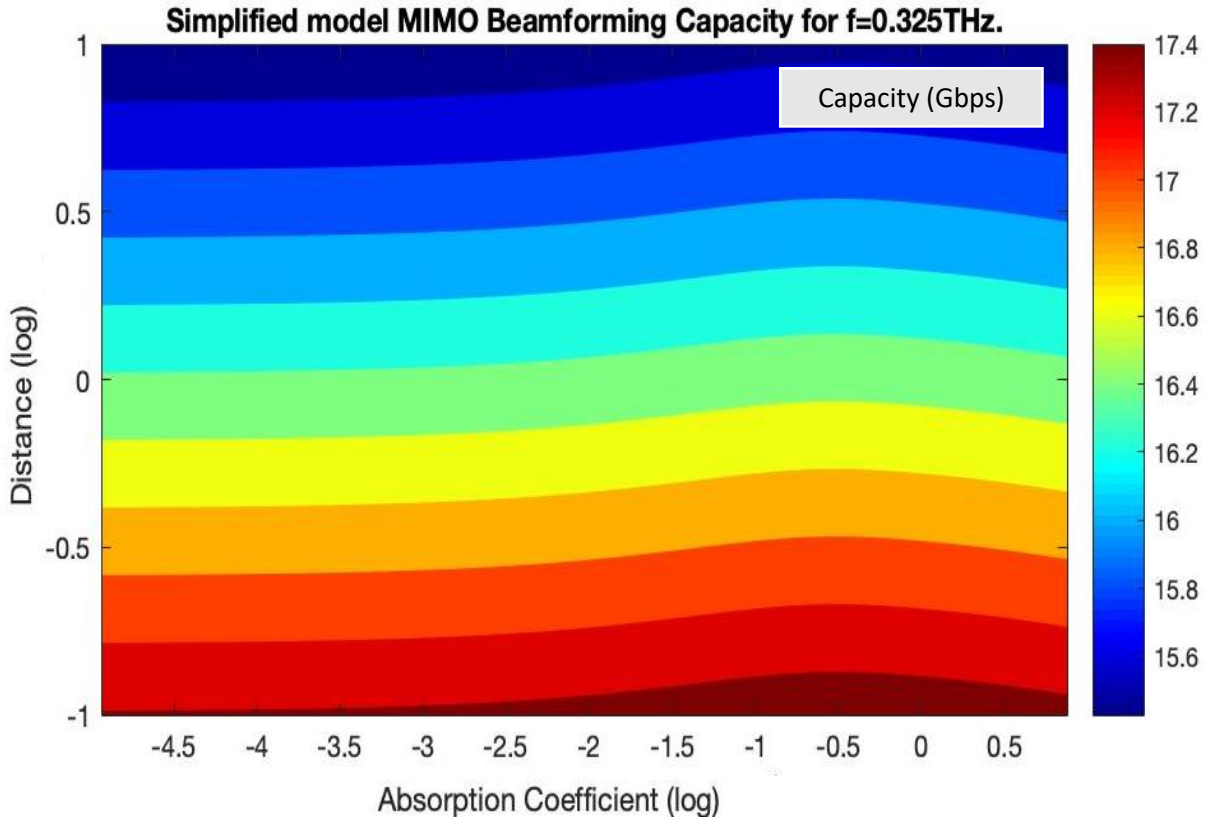

Figure 4.7 MIMO beamforming capacities plot with frequency 325 GHz which shows the relationship between the pre-determined space distance, ranging from 0.1 to 10 meters, and the absorption coefficient, according to Simplified model.

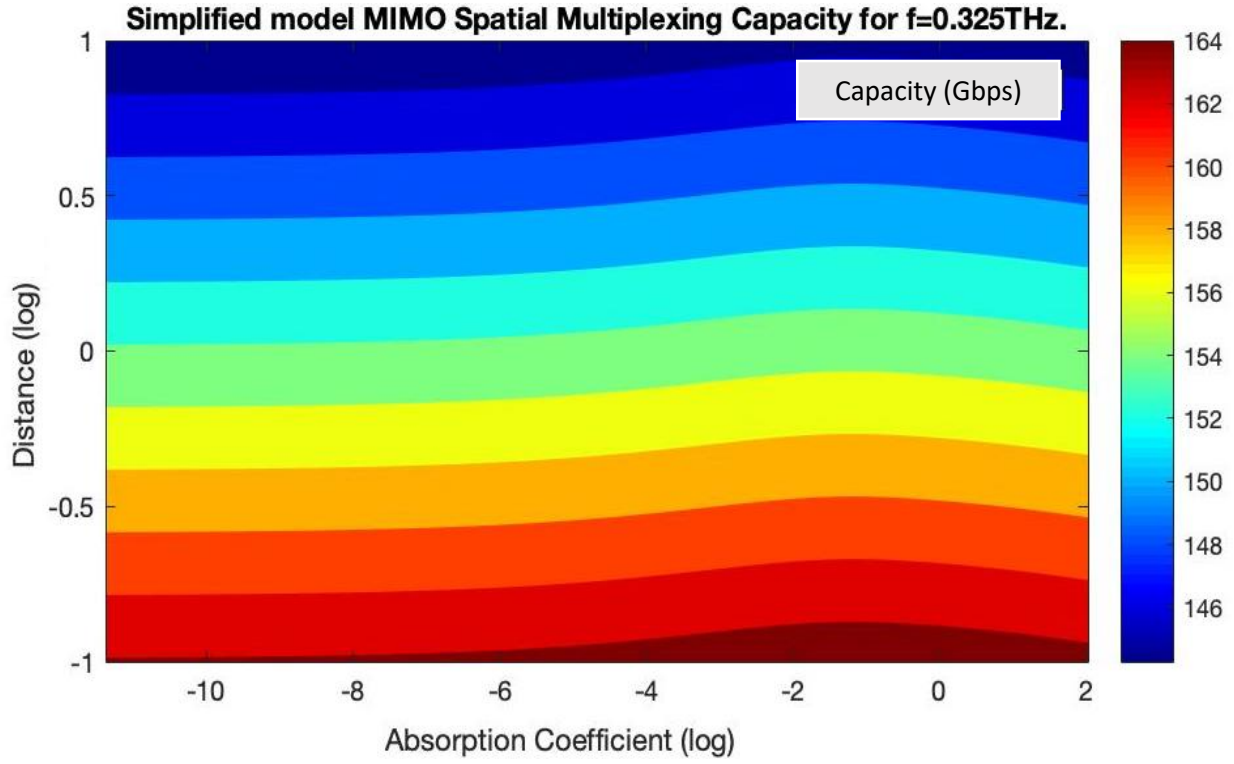

Figure 4.8 MIMO special multiplexing capacities plot with frequency 325 GHz which shows the relationship between the pre-determined space distance, ranging from 0.1 to 10 meters, and the absorption coefficient, according to Simplified model.

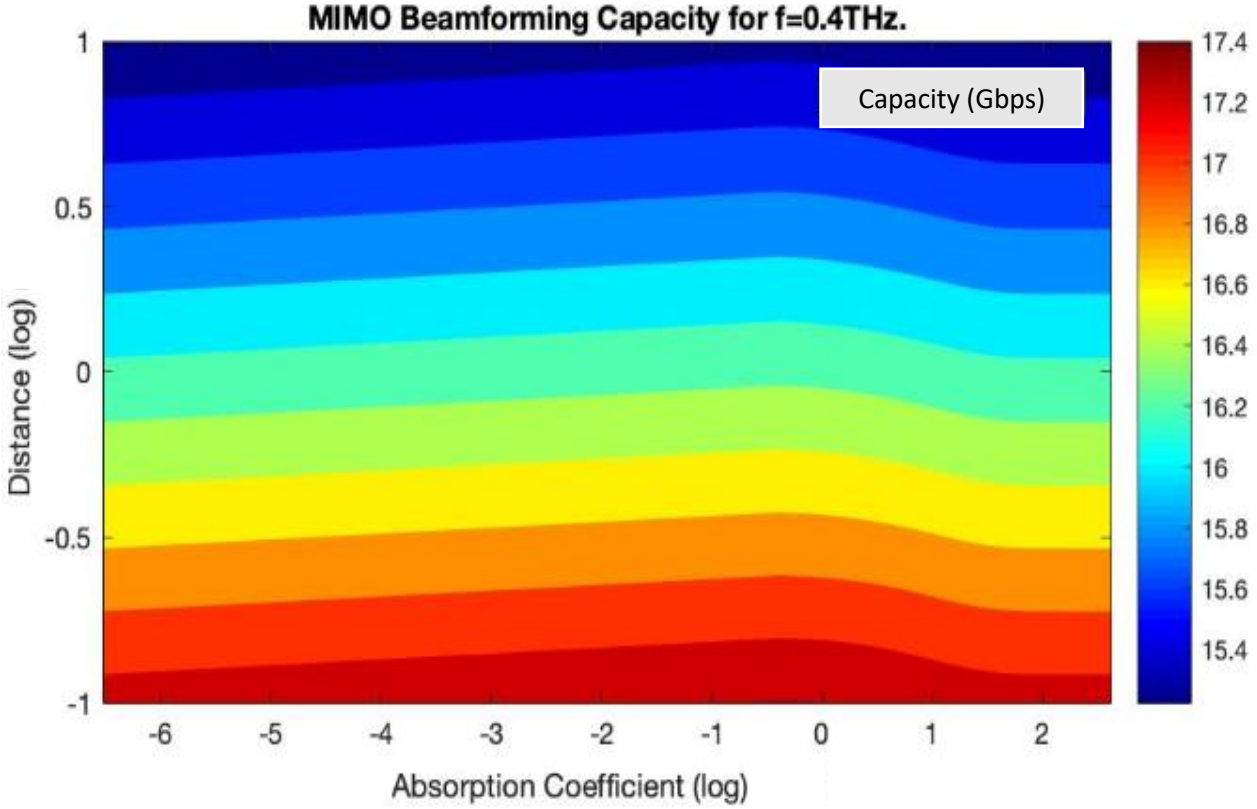

Figure 4.9 MIMO beamforming capacities plot with frequency 400 GHz which shows the relationship between the pre-determined space distance, ranging from 0.1 to 10 meters, and the absorption coefficient, according to Hosseini's model.

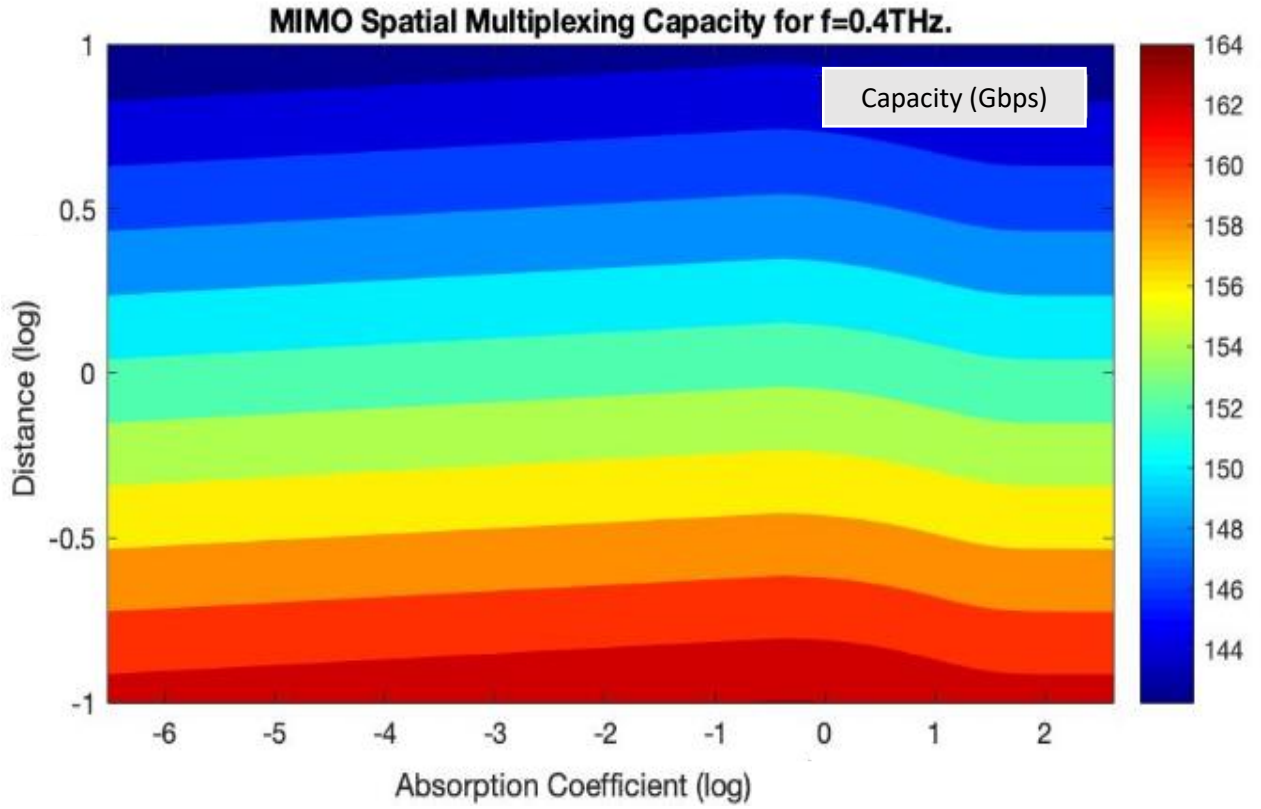

Figure 4.10 MIMO special multiplexing capacities plot with frequency 325 GHz which shows the relationship between the pre-determined space distance, ranging from 0.1 to 10 meters, and the absorption coefficient, according to Hosseini's model.

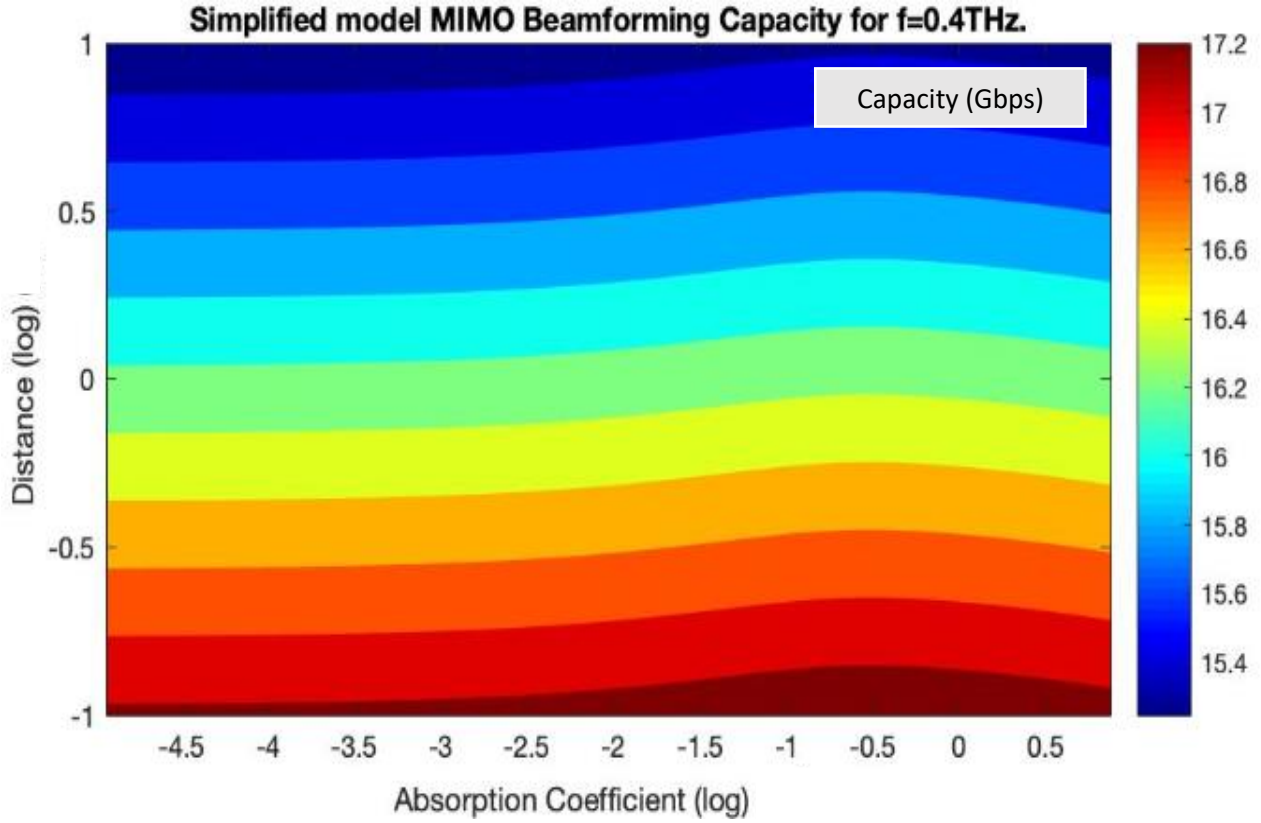

Figure 4.11 MIMO beamforming capacities plot with frequency 400 GHz which shows the relationship between the pre-determined space distance, ranging from 0.1 to 10 meters, and the absorption coefficient, according to Simplified model.

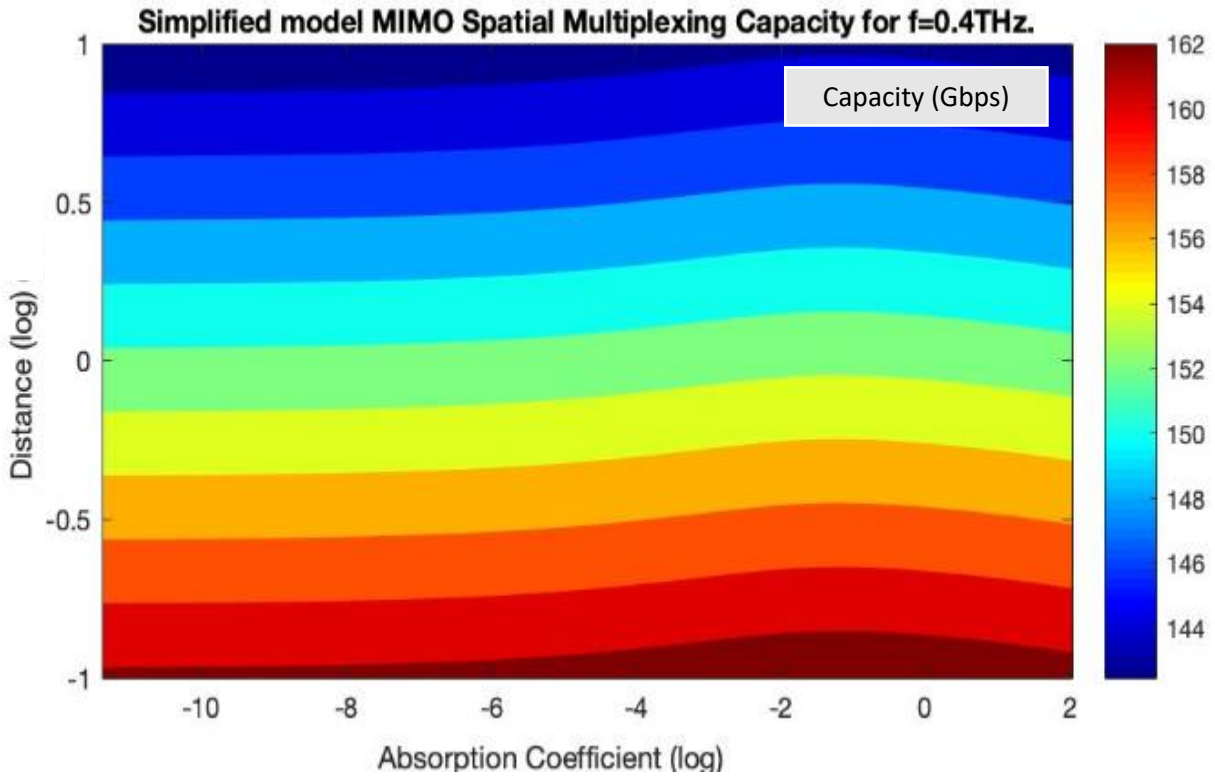

Figure 4.12 MIMO special multiplexing capacities plot with frequency 400 GHz which shows the relationship between the pre-determined space distance, ranging from 0.1 to 10 meters, and the absorption coefficient, according to Simplified model.

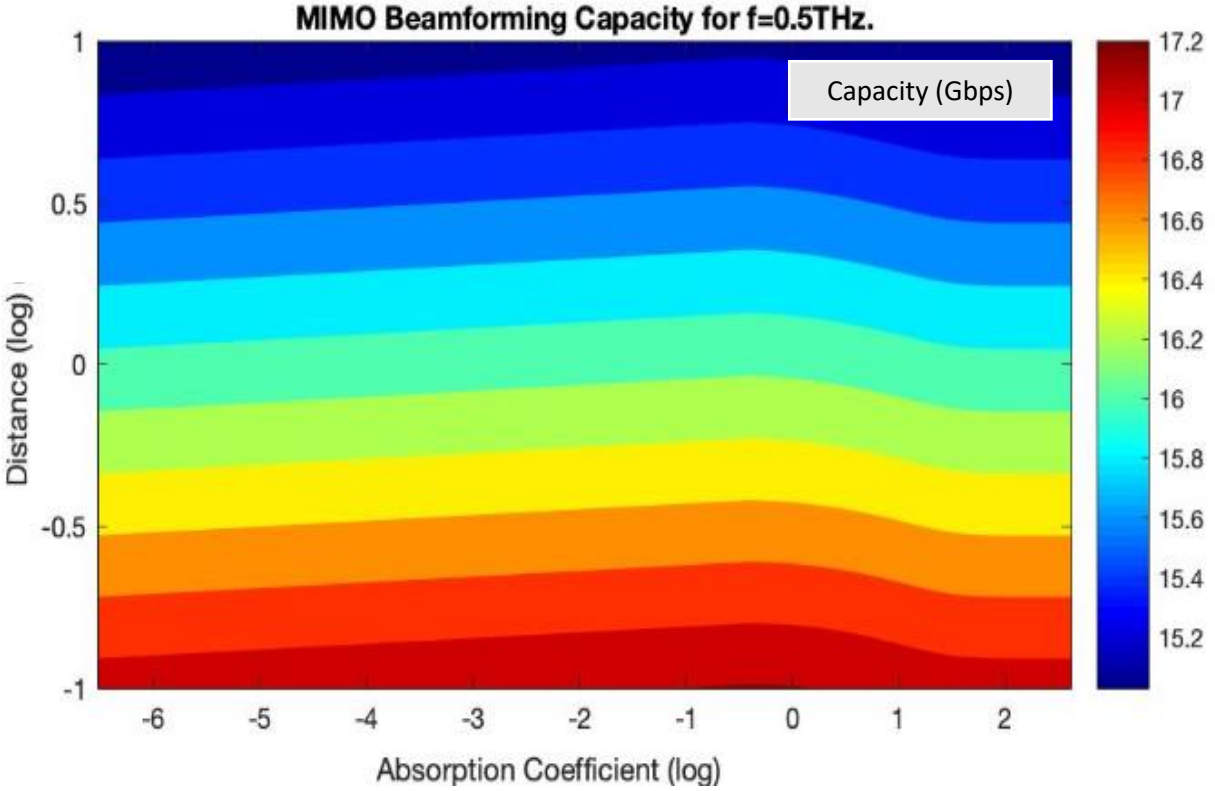

Figure 4.13 MIMO beamforming capacities plot with frequency 500 GHz which shows the relationship between the pre-determined space distance, ranging from 0.1 to 10 meters, and the absorption coefficient, according to Hosseini's model.

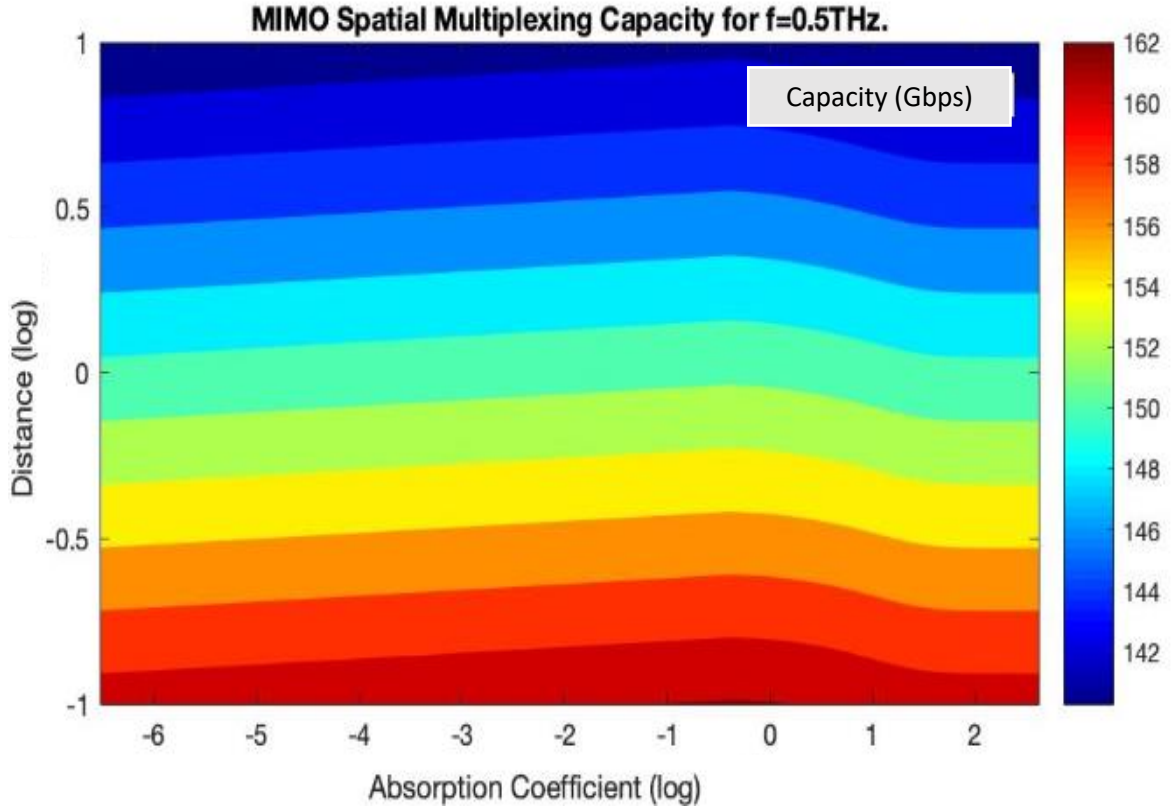

Figure 4.14 MIMO special multiplexing capacities plot with frequency 325 GHz which shows the relationship between the pre-determined space distance, ranging from 0.1 to 10 meters, and the absorption coefficient, according to Hosseini's model.

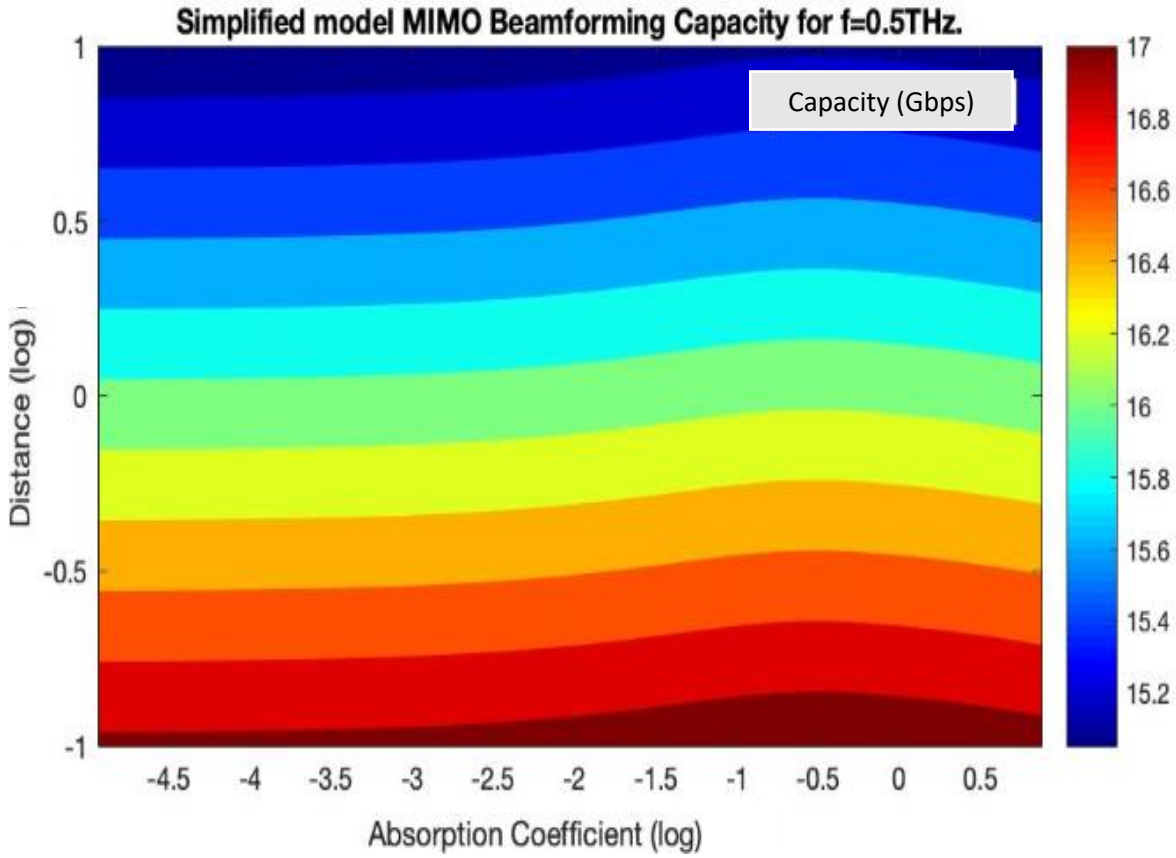

Figure 4.15 MIMO beamforming capacities plot with frequency 500 GHz which shows the relationship between the pre-determined space distance, ranging from 0.1 to 10 meters, and the absorption coefficient, according to Simplified model.

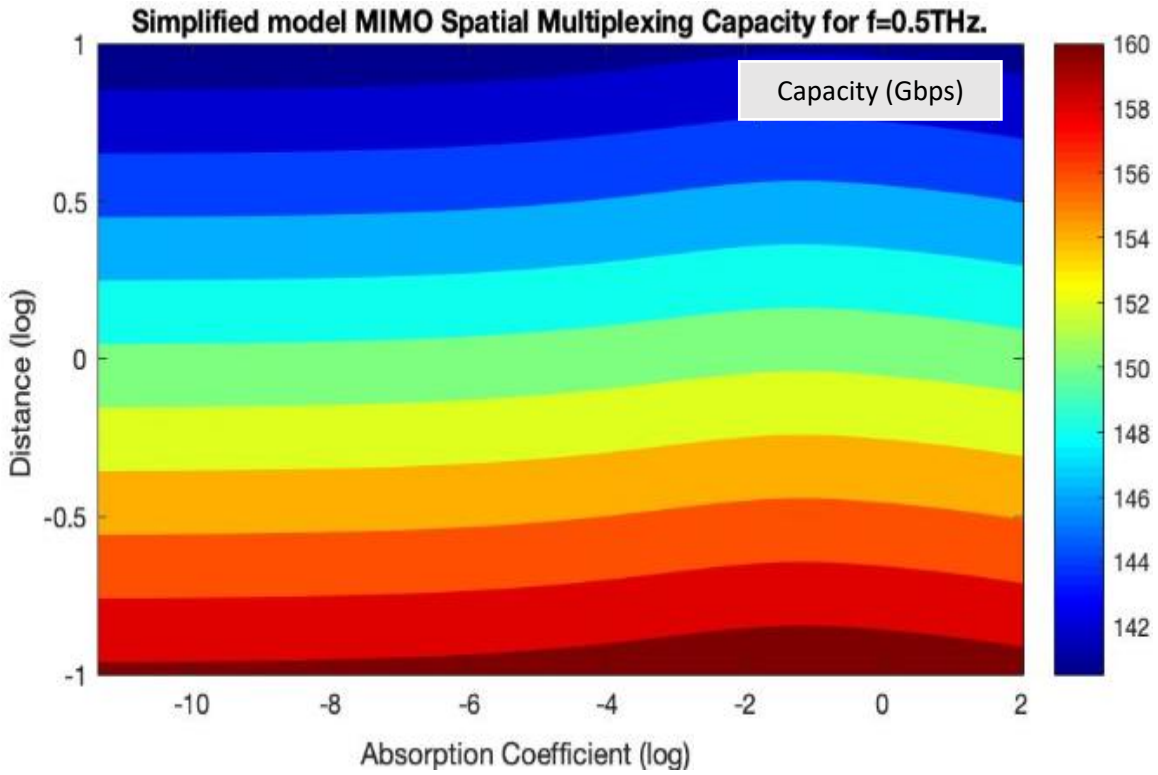

Figure 4.16 MIMO special multiplexing capacities plot with frequency 500 GHz which shows the relationship between the pre-determined space distance, ranging from 0.1 to 10 meters, and the absorption coefficient, according to Simplified model.

Firstly, the figures 4.5, 4.6, 4.7 and 4.8 are depicted for frequency 325 GHz, temperature $25^{o}\mathrm{C}$ and pressure 1 atm. The bandwidth is 15 GHz, which means that frequency oscillates between the values of 310 to 340 GHz. In Hosseini's model for absorption coefficient 10^{-2} and distance 1 m the MIMO beamforming capacity is 16 Gbps while the special multiplexing one is 150 Gbps. In the Simplified model for absorption coefficient 10^{-2} and distance 1 m the MIMO beamforming capacity is 16.3 Gbps whereas the special multiplexing one is 151 Gbps.

Secondly, the figures 4.9, 4.10, 4.11 and 4.12 are depicted for frequency 400 GHz, temperature $25^{o}\mathrm{C}$ and pressure 1 atm. The bandwidth is almost 20 GHz, which means that frequency oscillates between the values of 380 to 420 GHz. In Hosseini's model for absorption coefficient 10^{-2} and distance 2 m the MIMO beamforming capacity is 16.1 Gbps while the special multiplexing one is 151.2 Gbps. In the Simplified model for absorption coefficient 10^{-2} and distance 2 m the MIMO beamforming capacity is 15.9 Gbps whereas the special multiplexing one is 149.5 Gbps.

Thirdly, the figures 4.13, 4.14, 4.15, 4.16 are depicted for frequency 500 GHz, temperature $25^{o}\mathrm{C}$ and pressure 1 atm. The bandwidth is almost 40 GHz, which means that frequency oscillates between the values of 460 to 540 GHz. In Hosseini's model for absorption coefficient 10^{-2} and distance 1 m the MIMO beamforming capacity is 16.11 Gbps while the special multiplexing one is 151.5 Gbps. In the Simplified model for absorption coefficient 10^{-2} and distance 1 m the MIMO beamforming capacity is 16.15 Gbps whereas the special multiplexing one is 151.1 Gbps.

Several observations are made concerning the above figures, the main one being that the frequency selectivity due to the molecular absorption becomes more severe as the distance increases. It can also be seen that the absorption coefficient and distance show a downward trend. Additionally, the distance algorithm seems to have a relatively linear relationship with capacity. Another interesting conclusion is that the higher the frequency is, then the higher the capacities will be (figure 4.9). Moreover, the bandwidth of the transparency windows decreases as the transmission range increases.

Undoubtedly, the results obtained by these experiments are not unexpected. Indeed, there is an increase of capacity as the distance and absorption coefficient decrease. What is more, the capacities between the two models are similar for the same values of constants and they do not differ more than 1 Gbps. The error (φ) between the 2 models can be calculated by the following equation:

$$\varphi = \left| \frac{C_{Beamforming,\ Hosseini's\ model} - C_{Beamforming,\ simplified\ model}}{C_{Beamforming,\ simplified\ model}} \right| \times 100\%$$

For example, the error for the figure 4.9 with frequency 325 GHz, temperature $25^{o}\mathrm{C}$ and pressure 1 atm is negligible:

$$\varphi = \left| \frac{16 - 16.3}{16.3} \right| \times 100\% = \frac{0.3}{16.3} \times 100\% = 0.018 \times 100\% = 1.8\%$$

Finally, it should be mentioned that the K-factor and so, the absorption coefficient of the two models are different. This is because there is a difference in the water vapor content and thus, there is a difference in their values, since the equations for calculating the K-factor and absorption coefficient are related to the water content. As a result, the two models do not have same window for the absorption

coefficient but the same values this coefficient is required in order to compare of the capacities of the two models. That is why, in the absorption coefficient axis the values are multiplied with the factor 10^{-5} in the Simplified model, allowing the same observation window with absorption coefficient between $10^{-4.5}$ and $10^{-0.5}$.

4.5 Evaluation and Future Developments

Obviously, there is a superiority of the Simplified model compared to Hosseini's model. This is because is applied in a stricter THz band (i.e. 275 to 400 GHz) and the equations which have been developed for this model are more accurate and better regarding their arithmetic and numerical bounds. Consequently, this model is preferable for Wi-Fi and short distance networks but is inadequate as the distance is increases.

Further research could ideally focus in two main domains: the practical and the theoretical one. For the former one, new tractable deterministic wireless THz channel models for frequency ranges exceeding 450 GHz could be developed. For the later one, the perspective of developing totally stochastic wireless THz channel models should be considered. This kind of models could combine the effects of the deterministic path loss of the THz spectrum and possible stochastic characteristics common in wireless communications, such as multipath small-scale fading (mainly for indoor transmission scenarios) as well as shadowing and blockage due to objects within the transmission path. Furthermore, since THz links mainly rely on line-of-sight links the effect of misalignment fading among the transmitter's and receiver's beams should be taken into account in any possible stochastic channel model implementation.

5. References

[1] L. M. J. Federici, "Review of terahertz and subterahertz wireless communication," *Journal of Applied Physics,* vol. 107, no. 11, pp. 10.1063-10.13386413, March 2010.

[2] A. S. H. Shams, "Ptotonics, Fibers and THz Wireless Communications," *Optics and Photonics News,* vol. 28, no. 3, pp. 24-31, March 2017.

[3] M. D. M. H. S. A. Hoseini, "A New Look at MIMO Capacity in the Millimeter Wave," *GLOBECOM 2017-2017 IEEE Global Communications Conference,* December 2017.

[4] D. J. L. S. A. V. V. Y. Li, "A Survey of Millimeter Wave (mmWave) Communications for 5G: Opportunities and Challenges," *Wireless Networks,* vol. 21, no. 8, pp. 2057-2676, November 2015.

[5] M. D. M. H. S. A. Hoseini, "Massive MIMO Performance Comparison of Beamforming and Multiplexing in the Terahertz Band," *2017 IEEE Globecom Workshops (GcWkshps),* December 2017.

[6] M. D. D. L. Z. L. X. Yao, "What is the Optimal Network Deployment for a Fixed Density of Antennas?," *2017 IEEE Globecom Workshops (GcWshps),* December 2017.

[7] S. A. J. N. J. S. V. A. Goldsmith, "Capacity Limits of MIMO Systems," *IEEE Journal on Selected Areas in Communications,* vol. 21, no. 5, pp. 684-702, June 2003.

[8] H. Bengt, "Capacity of multiple-input multiple-output (MIMO) systems in wireless communications," 2002. [Online]. Available: https://www.ceid.upatras.gr/webpages/faculty/alexiou/ahts/other_pdf/6_mimo.pdf.

[9] A. B. R. G. J.-Y. C. E. Ghayoyla, "Capacity and Performance of MIMO Systems for Wireless Communications," *Journal of Engineering Science and Technology Review ,* vol. 7, no. 3, pp. 108-111, 2014.

[10] I. M. A. J. M. Jornet, "Channel Modeling and Capacity Analysis for Electromagnetic Wireless Nanonetworks in the Terahertz Band," *IEEE Transactions on Wireless Communications ,* vol. 10, no. 10, pp. 3211 - 3221, October 2011.

[11] "https://hitran.org/docs/definitions-and-units/," [Online].

[12] [Online]. Available: https://www.mathworks.com/discovery/channel-model.html.

[13] J. K. A.-A. A. B. J. L. A. A. M. J. E. N. Papasotiriou, "A new look to 275 to 400 GHz band: Channel model and performance evaluation," *IEEE International Symplosium on Personal, Indoor and Mobile Radio Communications,* September 2018.

[14] J. L. M. J. J. Kokkoniemi, "Simplified molecular absorption loss model for 275 – 400 gigahertz frequency band," *Institute of Electrical and Electronics Engineers,* 2018.

[15] R. E. E. O. A. Alduchov, "Improved magnus form approximation of saturation vapor pressure," *J. Appl. Meteor,* vol. 35, no. 4, pp. 601-609, April 1996.

[16] C. Haslett, Essentials of Radio Wave Propagation, Cambridge University Press, 2009.

[17] "https://hitran.org/links/," [Online]. Available: http://hitran.iao.ru/home.

[18] M. F. M. S. P. J. S. G. Lebrun, "MIMO Rician Channel Capacity and Asymptotic Analysis," *IEEE Transactions on Wireless Communications,* vol. 5, no. 6, pp. 1343-1350, June 2006.